



Kent Academic Repository

Robley Dixon, Lucas (2022) *Elucidating the difference in structure and enzymatic activity of the homologues GSTO1 and CLIC1*. Master of Science by Research (MScRes) thesis, University of Kent,.

Downloaded from

<https://kar.kent.ac.uk/100272/> The University of Kent's Academic Repository KAR

The version of record is available from

This document version

UNSPECIFIED

DOI for this version

Licence for this version

CC BY (Attribution)

Additional information

Versions of research works

Versions of Record

If this version is the version of record, it is the same as the published version available on the publisher's web site. Cite as the published version.

Author Accepted Manuscripts

If this document is identified as the Author Accepted Manuscript it is the version after peer review but before type setting, copy editing or publisher branding. Cite as Surname, Initial. (Year) 'Title of article'. To be published in **Title of Journal**, Volume and issue numbers [peer-reviewed accepted version]. Available at: DOI or URL (Accessed: date).

Enquiries

If you have questions about this document contact ResearchSupport@kent.ac.uk. Please include the URL of the record in KAR. If you believe that your, or a third party's rights have been compromised through this document please see our [Take Down policy](https://www.kent.ac.uk/guides/kar-the-kent-academic-repository#policies) (available from <https://www.kent.ac.uk/guides/kar-the-kent-academic-repository#policies>).



University of Kent

MSc by Research Thesis

Elucidating the difference in structure and enzymatic activity
of the homologues GSTO1 and CLIC1.

Author – Lucas Robley Dixon

Degree – MSc-R Biochemistry, School of Biosciences

Word Count (Excluding References) – 10,927

Page Count - 63

Thesis Advisor – Dr Jose Luis Ortega-Roldan

December 2021

1 Declaration

No part of this thesis has been submitted in support of an application for any degree or qualification of the University of Kent or any other University or institute of learning.

Lucas Robley Dixon

September 2022

2 Acknowledgements

I would like to take this opportunity to thank my MSc by Research supervisor – Dr Jose Luis Ortega-Roldan for his academic guidance, support and patience. Whilst it has been a challenging year due to the corona virus pandemic he made the lab an extremely enjoyable, exciting and interesting place to work.

I would also like to thank Dr Gary Thompson for always being available to help with any issues I had with NMR as well as his training seminars. My thanks also to Dr Christopher Mulligan and members of his lab for teaching me how to use the QPCR in order to perform ThermoFluor experiments. I would also like to thank the technical staff for helping with any issues or questions I had with the departmental equipment.

Finally, I would like to thank the members of Ortega lab Joseph Cassar, Victoria Cheung and Eleanor Towler who are the people I spent the most time with over the last year and have made my masters a great experience. Particular thanks goes to Joseph Cassar who shared his knowledge, answered my unending amount of questions, helped guide me through the year and was always there to talk to.

3 Contents

| | |
|--|----|
| 1 Declaration..... | 2 |
| 2 Acknowledgements..... | 3 |
| 3 Contents..... | 4 |
| 4 List of Figures..... | 7 |
| 5 List of Tables..... | 9 |
| 6 List of Abbreviations..... | 10 |
| 7 Abstract..... | 11 |
| 8 Introduction..... | 12 |
| 8.1 Glutathione-s-transferase general background..... | 12 |
| 8.2 Glutathione-s-transferase structure..... | 12 |
| 8.3 Role and cellular function of Glutathione-s-transferase..... | 13 |
| 8.4 Glutathione S-transferase omega-1..... | 15 |
| 8.5 Chloride intracellular channel protein general background..... | 17 |
| 8.6 Chloride intracellular channel protein structure..... | 18 |
| 8.7 Chloride intracellular channel protein roll, cellular function and membrane insertion..... | 19 |
| 8.8 Chloride intracellular channel protein 1..... | 20 |
| 8.9 Project Aims..... | 22 |
| 9 Materials and Methods..... | 23 |
| 9.1 Transformations..... | 23 |

| | |
|--|-----------|
| 9.2 Cell Growth..... | 23 |
| 9.3 Protein Purification..... | 24 |
| 9.4 Multiple sequence alignment..... | 25 |
| 9.5 Structural alignment..... | 25 |
| 9.6 SAXS..... | 25 |
| 9.7 B Factor analysis..... | 26 |
| 9.8 Intramolecular bond analysis..... | 26 |
| 9.9 Thermofluor analysis..... | 27 |
| 9.10 NMR..... | 27 |
| 9.11 PEPTIDE SYNTHESIS AND PURIFICATION..... | 27 |
| 10 Results..... | 29 |
| 10.1 Sequence and structural alignments of GSTO1 and CLIC1..... | 29 |
| 10.2 Elucidating the in-Solution Structures and Conformational Dynamics of GSTO1 and CLIC1 using SAXS..... | 32 |
| 10.3 Measuring protein flexibility, subunit-subunit interactions and intramolecular dynamics for GSTO1 and CLIC1..... | 34 |
| 10.4 Comparison of the GSH binding site on GSTO1 and CLIC1..... | 43 |
| 10.5 Analysis of GSTO1 GSH binding site when complexing with GSH saturated peptide.. | 48 |
| 11 Discussion..... | 50 |
| 11.1 Differences in X-ray crystal structure..... | 50 |
| 11.2 Elucidating the in-Solution Structures and Conformational Dynamics of GSTO1 and CLIC1 using SAXS..... | 51 |

| | |
|---|-----------|
| 11.3 Structural disorder and intramolecular bonding in GSTO1 and CLIC1..... | 52 |
| 11.4 Comparison of the GSH binding site on GSTO1 and CLIC1..... | 53 |
| 11.5 The Footloop hypothesis..... | 54 |
| 11.6 The H9 helix hypothesis..... | 56 |
| 11.7 Limitations..... | 56 |
| 11.8 Further research..... | 56 |
| 12 Conclusions..... | 57 |
| 13 References..... | 58 |

4 List of Figures

| | |
|---|----|
| Figure 1: Shows a sequenced-based phylogenetic tree..... | 13 |
| Figure 2: Overview of enzymatic detoxification..... | 14 |
| Figure 3: The 1eem crystal structure of GSTO1..... | 15 |
| Figure 4: The 1k0m crystal structure of CLIC1..... | 19 |
| Figure 5: A sequence alignment between Human GSTO1 and Human CLIC1. | 30 |
| Figure 6: A structural alignment of GSTO1 and CLIC1..... | 31 |
| Figure 7: A graph showing experimental scattering data plotted against the theoretical SAXS curve of the crystal structure..... | 32 |
| Figure 8: P(r) graphs for GSTO1 and CLIC1..... | 33 |
| Figure 9: A graph plotting all B factors for each amino acid in CLIC1's (PBD ID: 1k0m) monomer A and B..... | 35 |
| Figure 10: B factor visually displayed on CLIC1's crystal structure (PBD ID: 1k0m)..... | 35 |
| Figure 11: A graph plotting the B factor for each amino acid in GSTO1 (PBD ID: 1eem)..... | 36 |
| Figure 12: B factor visually displayed on GSTO1's crystal structure (PBD ID: 1eem)..... | 37 |
| Figure 13: NMR spin relaxation of CLIC1..... | 38 |
| Figure 14: Shows the Thermofluor melt curve plot for soluble wild type CLIC1 and un-cleaved His-tagged CLIC1..... | 42 |
| Figure 15: Shows the Thermofluor melt curve plot for GSTO1 in various buffers..... | 42 |
| Figure 16: BTROSY spectrums of GSTO1 at 181uM, 308K, pH 7.4, 20mM NaCl, 20mM..... | 44 |
| Figure 17: SOFAST spectrums of CLIC1 at 181uM, 308K, pH 7.4, 20mM NaCl, 20mM..... | 45 |
| Figure 18: Chemical shifts (ppm) plotted against amino acid number for CLIC1..... | 46 |

Figure 19: A visual representation of chemical shift in CLIC1's (PBD:1k0m) amino acids when binding to GSH.....47

Figure 20: BTROSY spectrums of GSTO1 at 145uM, 308K, pH 7.4, 20mM NaCl, 20mM.....49

5 List of Tables

Table 1: Intramolecular bonds and interactions predicted in CLIC1 crystal structure

(PBD:1k0m).....40

Table 2: Intramolecular bonds and interactions predicted in GSTO1 crystal structure

(PBD:1eem).....40

6 List of Abbreviations

GST - Glutathione S-Transferase

GSTO1 - Glutathione S-Transferase Omega 1

CLIC – Chloride intracellular channel protein

CLIC1 - Chloride intracellular channel protein 1

GSH- Glutathione

NMR – Nuclear magnetic resonance

SAXS – Small angle X-ray scattering

ROS – Reactive oxygen species

7 Abstract

The Glutathione-S-Transferase superfamily are a widespread collection of enzymes that catalyse glutathione conjugation to various compounds as well as wide range of other functions. Chloride intracellular channel protein 1 is known to be a structural homologue of Omega glutathione-S-transferase 1 an enzyme belonging to the omega subclass of this superfamily. GSTO1 is a soluble enzyme thought to have a role in the glutathionylation cycle whereas CLIC1 belongs to a special class of metamorphic proteins. CLIC1 has the ability to switch from its soluble form which is homologous to GSTO1 to a membrane bound form that oligomerises to create an ion channel. The mechanism for this is insertion is not well understood. By comparing the crystal and in-solution structures of these two proteins some notable differences were discovered. With the help of SAXS the in-solution structure of CLIC1 was found not to match that of its X-ray crystal structure unlike GSTO1. Further analysis of the proline rich 'footloop' found in CLIC1 also highlighted it as an area that could potentially act as a hinge and allow for conformational change in CLIC1. This difference in structure between the two proteins could explain how CLIC1 can change shape and GSTO1 cannot. Analysis of their enzymatic properties was also carried out but the data gathered was less conclusive due to the lack of assignment for the GSTO1 protein.

8 Introduction

8.1 Glutathione-s-transferase general background:

Omega glutathione-S-transferase 1 (OGST1) is a protein belonging to the Glutathione-S-Transferase superfamily¹, a widespread collection of enzymes with varied functions. The superfamily can be further subdivided into three groups: cytosolic, mitochondrial and microsomal¹⁻⁴. Microsomal since their discovery have been reclassified as, membrane-associated proteins in eicosanoid and glutathione (MAPEG)⁵. Cytosolic GSTs are the largest subfamily and are divided into classes based on their structure, these classes are alpha, beta, delta, epsilon, zeta, theta, mu, nu, pi, sigma, tau, phi, and omega⁵. The mitochondrial GSTs are in class kappa. And the MAPEG or microsomal GSTs consists of subgroups designated I-IV⁵. Cytosolic GSTs within the same class have greater than 40% sequence identity and between classes no more than 25% sequence identity⁵. Figure 1 below shows a sequenced-based phylogenetic tree containing a member from each class of GST's found in humans and a the closely related CLIC family of proteins (CLIC1-6). The tree shows the close evolutionary relationship between the cytosolic GST's (GSTM1, GSTA1, GSTP1, GSTO1, MAAI and GSTT1) The mitochondrial GST (GSTK1) has a slightly closer relationship than that of the MAPEG GST (MGST1) to the cytosolic class. This is unsurprising as cytosolic and mitochondrial GST have a much more similar fold which will be elaborated on below. This tree also shows the relationship between the GST and CLIC family of proteins some of which are close structural homologues.

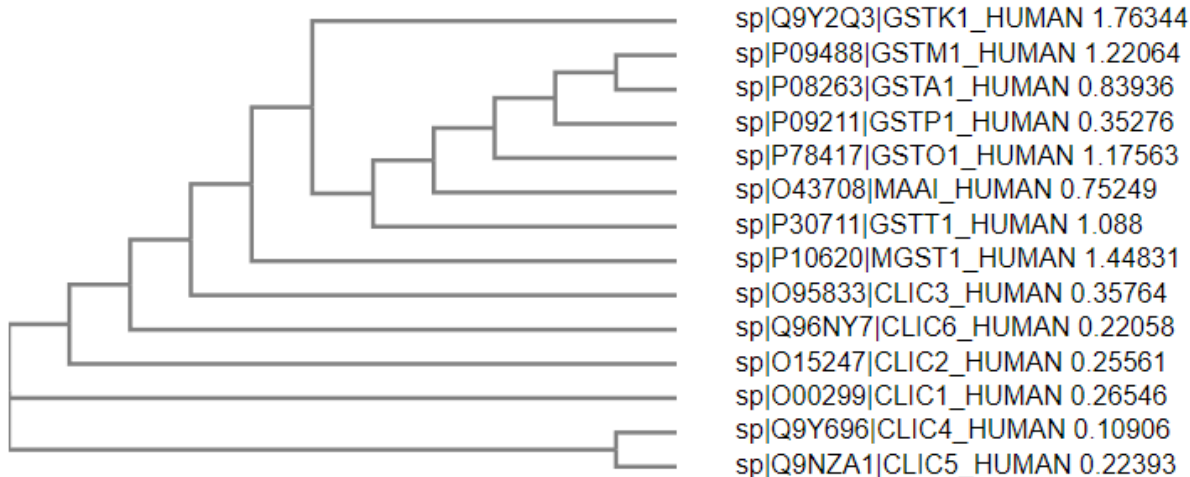


Figure 1: Shows a sequenced-based phylogenetic tree.

This sequenced-based phylogenetic tree shows the evolutionary relationship between the human proteins CLIC1-6 and a member of each class of GST's found in humans.

8.2 Glutathione-s-transferase structure:

The cytosolic and mitochondrial GSTs have a deep evolutionary history and therefore have some consistencies in their fold^{6,7}. However, the same cannot be said for the MAPEG class of GSTs⁸. Mitochondrial and cytosolic GSTs can also form dimers⁵. The porcine pi-class enzyme (pGSTP1-1) was the first cytosolic GST to have its structure elucidated. It also contains all the hallmark features of the cytosolic GST subgroup, for this reason it has been used as the standard to compare to the other isoenzymes⁹. These features are an N-terminal thioredoxin-like domain (with $\beta\alpha\beta\alpha\beta\alpha$ topology) and a C-terminal domain composed of α -helices. The glutathione binding site or 'G-site' is located in the thioredoxin-like domain for both cytosolic and membrane GSTs³.

8.3 Role and cellular function of Glutathione-s-transferase:

The classical role of the first discovered GSTs was detoxification of the cell by nucleophilic substitution where the GST catalysed the addition of glutathione (GSH) to exogenous compounds that contain an electrophilic nitrogen, carbon, or sulphur atom¹⁰⁻¹³. Many of the GST family are expressed in the liver^{14,15} which is consistent with their role in detoxification. GSTs role in cell metabolism is vital as, in order for a cell to maintain proper function and stay healthy it must be capable of coping with and regulating pressures both internal and external. Toxins that are either endogenously produced or xenobiotic compounds must be neutralised. A build-up of one such type of toxin causes oxidative stress. Oxidative stress is caused by an elevated intracellular level of reactive oxygen species (ROS), examples of which are endogenously produced peroxides and superoxides^{16,17}. ROS can be produced from mitochondrial oxidative metabolism, cytoplasmic enzyme systems, endoplasmic reticulum-bound enzymes and the surface of the plasma membrane^{18,19}. An imbalance of ROS can be caused by a variety of factors such as UV exposure, hyperoxia, inflammation or heat^{17,20}. High levels of ROS in cells have been linked to a number of different pathologies and can cause damage to lipids, DNA and proteins. Therefore, cell detoxification mechanisms are vital for cell health²¹.

Cell detoxification using enzymes is broken down into three phases. Phases I and II work to detoxify the compound by making it more water soluble²². Phase III which actively transports the toxin out of the cell via transmembrane ATPase such as the GS-X pump²³. GSHs are phase II enzymes with their main function being to catalyse conjugation of GSH to the toxin. This prevents the toxin re-entering the cell after it has been actively transported

out, as the toxin-GSH conjugate is too hydrophilic to freely diffuse through the membrane^{24,25}. GSTs also play a role as regulators for the MAP kinase pathway^{26,27}. They play a key role regulating protein-protein interactions. One such example is GST π acting as an endogenous inhibitor of c-Jun N-terminal kinase 1 (JNK1)²⁸. This kinase is involved in stress response, apoptosis, and cellular proliferation²⁹.

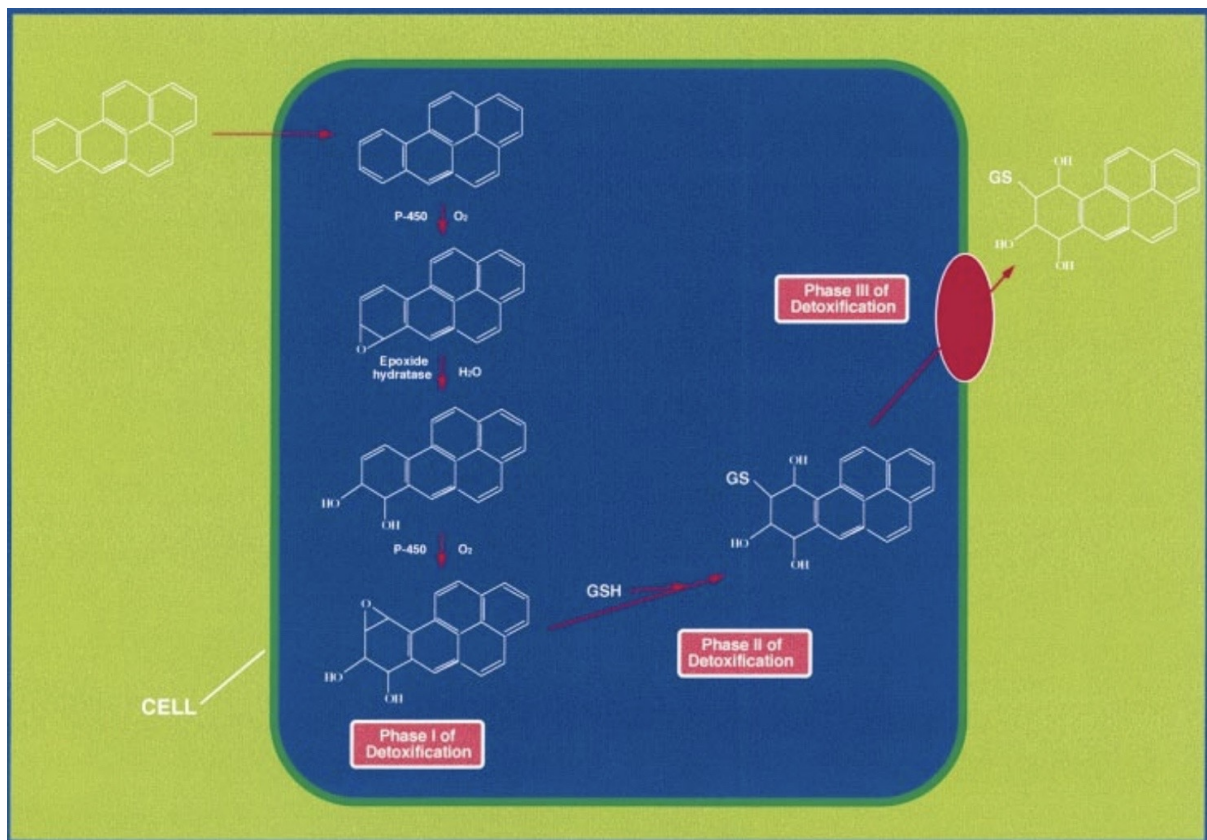


Figure 2: Overview of enzymatic detoxification.

Reprinted from “Structure, function and evolution of glutathione transferases: implications for classification of non-mammalian members of an ancient enzyme superfamily” by D. Sheehan, 2001, *Biochemical Journal*, 360(1), 2. Copyright [2001] by the Biochemical Society.

8.4 Glutathione S-transferase omega-1:

Toxins are not the only molecules in the cell that can be bonded with GSH, it has been found that when a cell is undergoing oxidative stresses many protein thiols are 'capped' with GSH forming a mixed disulphide. This protects the electrophilic atom in the thiol from irreversible oxidation by ROS. After the cell had dealt with the oxidative stress the disulphide can be reduced, and the protein can resume normal function^{30,31}. It is here where GSTO1 is believed to function³². GSTO1 is not as well understood as many of its family, Omega class GSTs were first discovered by bioinformatics in 2000 and are the most recent family of GSTs to be identified^{1,33}. It is one of two actively transcribed omega class GSTs and in humans it is located on the long arm of chromosome 10, the Unigene map reference is 10q25.1. The gene is 12.5kb long and contains 6 exons³⁴. GSTO1 is expressed widely throughout mammalian tissue. Human GSTO1 is 241 amino acid long and forms a dimer, the monomer of GSTO1 is 27.6kDa in size^{1,33}.

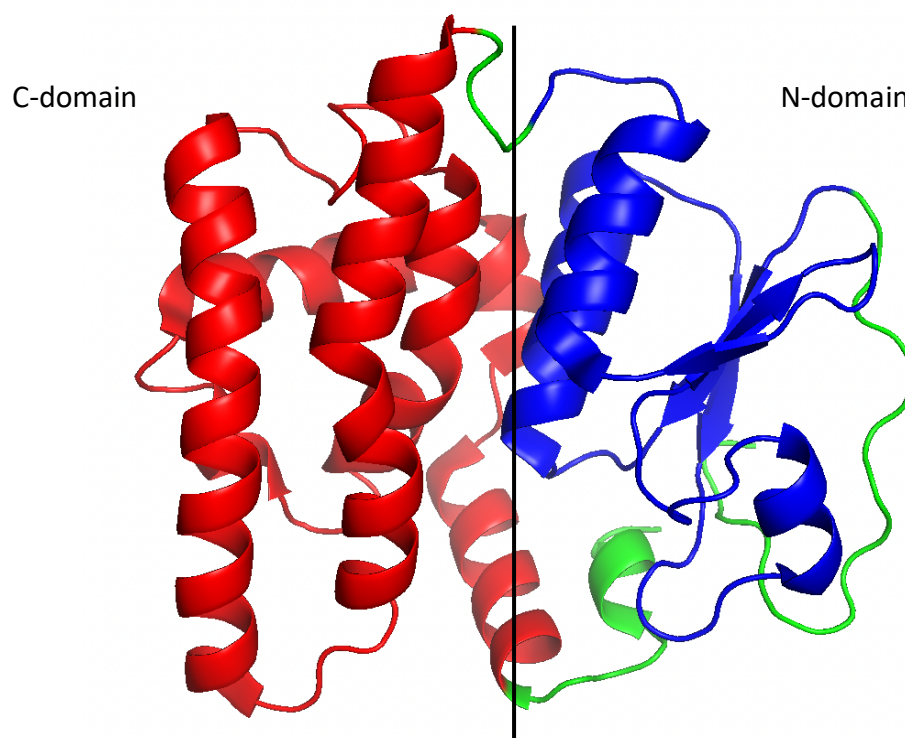


Figure 3: The 1eem crystal structure of GSTO1. GSTO1 shown above with a black line separating the C and N-domains. With the GST N-terminal being shown in blue (22-101) and the GST C-terminal shown in red (106-230)

As stated above Omega GSTs have a lower than usual sequence identity compared to other GST classes at 20%. Despite this it still exhibits the GST fold. Unlike other GSTs GSTO1 has proline rich N-terminal extension that is 19-20 residues long and a C-terminal extension^{1,33}. These extensions interact to form a novel structural feature that has not been seen in the other GST classes³⁵. A PXXP motif is found in the N-terminal extension, this motif provides the core sequence for recognition by a SH3 domain, this has possible implications in potential protein-protein interactions³⁶. One last major structural difference is in GSTO1 catalytic site. The typical serine/tyrosine atom found in the catalytic site of other GSTs is replaced by a cystine in human GSTO1. This has large implications in potential functions for the enzyme as it changes the type of reactions GSTO1 can catalyse^{1,33}.

The inter-subunit interface is also more open than in other classes of GSTs with the buried area only being 1960 Å² whereas other GST dimers have values ranging from 1900-2600 Å². This interface is also largely full of non-polar interactions^{1,33}.

The function of GSTO1 is not very well defined, although there have been several suggested functions. One such function is a role in the glutathionylation cycle as GSTO1 catalyses several reactions linked to this cycle and displays dehydroascorbate reductase, S-(phenacyl)glutathione reductase activities as well as glutaredoxin activity³². Meaning GSTO1 may have the ability to either 'cap or 'uncap' vulnerable protein thiol groups when a cell is undergoing oxidative stresses. The relatively open hydrophobic bonding site is big enough to fit polypeptide chains further supporting this theory¹. A chloride ion channel named CLIC1 is a structural homologue to GSTO1³⁷, as CLIC1 can oligomerise to form an ion channel³⁸, Several experiments were carried out to test if the same was true for GSTO1. This turned out not to be the case³⁷. However, another potential function of GSTO1 was discovered.

GSTO1 was found to inhibit cardiac muscle ryanodine receptor (RyR2) activity, but in contrast increase skeletal muscle ryanodine receptor (RyR1) activity^{37,39}. Ryanodine receptors are calcium channels and the inhibition effect depended on the GST being catalytically active. When the cystine residue in the active site was mutated into an alanine this effect was no longer observed. This may suggest a role for Omega GSTs in protecting cells from apoptosis caused by Ca²⁺ mobilization from intracellular stores.

8.5 Chloride intracellular channel protein general background:

Chloride intracellular channel protein 1 or CLIC1 is a protein belonging to the CLIC family a group of six evolutionarily conserved proteins in humans consisting of CLIC1⁴⁰, CLIC2⁴¹, CLIC3⁴², CLIC4^{43,44}, CLIC5⁴⁵ and CLIC6.⁴⁶ All proteins in the CLIC family share a high homology with one another and are in a rare classification of metamorphic proteins⁴⁷, meaning they adopt different folded conformations for the same amino acid sequence in native conditions⁴⁸. Unlike some other proteins namely prions that can change conformations this process for metamorphic proteins is reversible. The CLIC family of proteins exist in two states a globular soluble form which has high structural homology to the GST superfamily of proteins, and an integral membrane bound form that oligomerise to create ion channels in the membrane⁴⁹. The CLIC family of proteins is expressed in the cell membrane, cytoplasm, nuclear membrane and nucleoplasm. It can also be found in the lysosome, endoplasmic reticulum, and secretory vesicles⁵⁰⁻⁵².

8.6 Chloride intracellular channel protein structure:

As stated above the CLIC family of proteins have metamorphic properties in CLICs case meaning they adopt two distinct structures. The cytosolic or soluble crystal structure that CLIC forms is very similar to that of the GST family, the thioredoxin-like domain is present in CLICs N-domain as well as the alpha helices in the C-domain^{53,54}. CLIC also binds GSH, with the G site found in CLICs thioredoxin-like domain⁵⁵. There is an especially close link between CLIC1 and GSTO1 soluble crystal structure³⁷ which will be expanded upon further below. Far less is known about the structure of CLIC in its integral membrane bound form. This is due to the fact that it is very hard to get membrane proteins to crystallise and when removed from the membrane CLIC immediately return to their soluble form. Other methods that may be used for determining structure such as cryo-EM have difficulties as the CLIC proteins are currently too small for the technique⁵⁶. Solid state NMR has been used with increasing success over the last few decades to fill in this gap determining membrane bound structures⁵⁷ however, there are still limitations and so far, it has not been able to assist with CLIC. It is thought the segment of the protein that forms the transmembrane section of the ion channel is the thioredoxin-like domain of the N-domain⁵⁸.

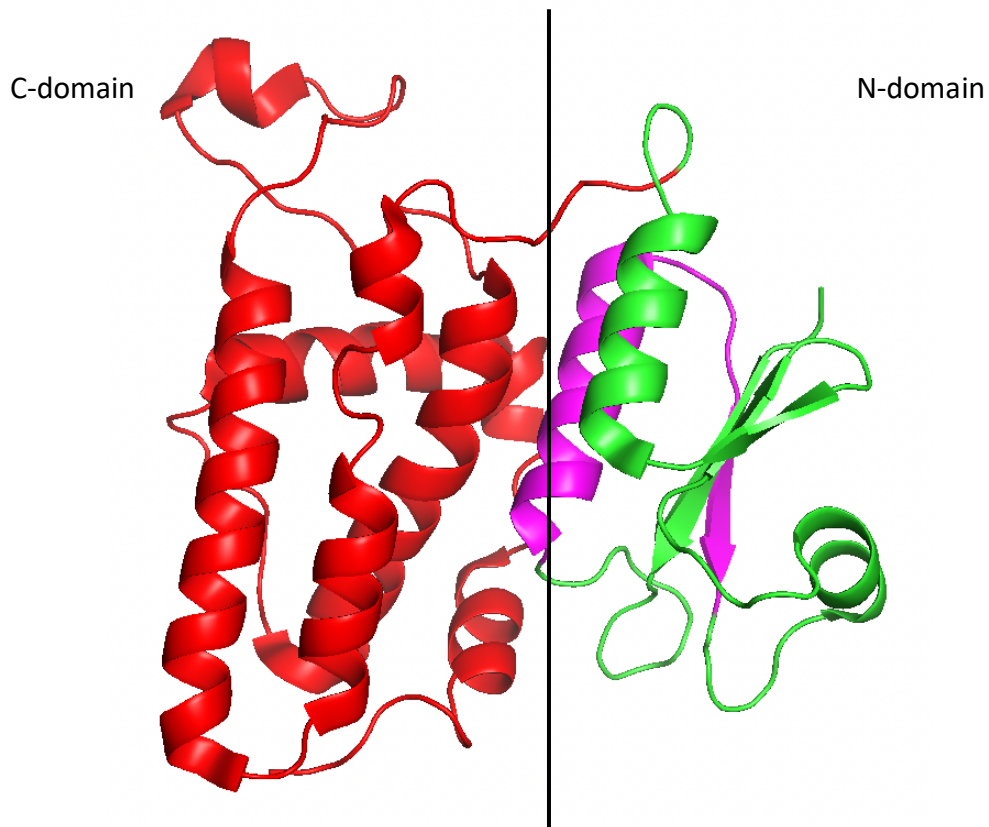


Figure 4: The 1k0m crystal structure of CLIC1. CLIC1 shown above with a black line separating to C and N-domains. The GST C-terminal domain is shown in red (93-233), the suggested putative transmembrane domain shown in purple (24-46) and the N-terminal region shown in green (6-92).

8.7 Chloride intracellular channel protein role, cellular function, and membrane insertion:

Elucidating the role of the CLIC has proven to be difficult due to what is thought to be functional redundancy in knock out model systems. Despite this knock out model systems in mice have been established for CLIC1⁵⁹, CLIC4⁶⁰ and CLIC5⁶¹. From these knock-out systems various roles in regulation have been suggested including cell growth, cell division, cell apoptosis, formation of stereocilia and acidification of intracellular organelles.

As stated above it is known that the CLIC family of proteins oligomerise in order to create ion channels. The mechanism that causes CLICs to insert into the membrane has been at the forefront of recent research, with many potential triggers being put forth such as signals from redox states, pH change or membrane composition^{62,63}. Some recent research has evidence strongly suggesting that the switch is caused by divalent cations binding⁶⁴.

8.8 Chloride intracellular channel protein 1:

The most studied member of the CLIC family is CLIC1. Located on chromosome 6 Unigene map reference 6p21.33 it is comprised of 241 amino acids and is 26.932kDa in mass^{37,51,53}. CLIC1 is expressed all throughout the human body and is especially abundant in cardiac or skeletal muscle⁵⁰. Like the rest of the CLIC family its cellular function is not well understood however it has been associated with roles in the cell cycle, regulation of electrical excitability amongst others. CLIC1 is found in the cytoplasm, cell membrane, nucleus and nuclear membrane^{37,50,51,53,58}.

The structure of CLIC1s soluble form is well known and is a structural homologue of GSTO1. Despite the low sequence identity between the two (19.1%) the sequence of CLIC1 is still clearly compatible with the known GST fold, along with the conserved cystine residue in the binding site of both proteins. CLIC1 like GSTO1 has a thioredoxin-like fold in its N-domain and a C-domain made up of all alpha helices. These two domains are linked via a proline rich loop, which along with the position of the H9 helix being slightly shifted are the only major differences between the structure of CLIC1 and GSTO1³⁷. Like the rest of its family CLIC1s

membrane bound structure is not known however, it has been shown to form a tetramer when bound to the membrane⁶⁵. It is not clear whether CLIC1 inserts into the membrane as a tetramer or forms a tetramer once inserted into the membrane. The absence of a leader sequence or obvious hydrophobic segment to enable membrane insertion has made it difficult to study membrane insertion⁶⁶. Combined with the fact that as soon as CLIC1 is removed from the membrane it reverts to its soluble form instantly means there is still no established mechanism of insertion. Historically it was suggested that insertion was triggered by oxidative conditions⁶². However, more recent research suggests that this is not the case^{64,65}. Other theories pointed towards cholesterol or pH being a factor in insertion. A hydrophobic surface in CLIC1 made up of residues 24-46 has been suggested as being a putative transmembrane domain which could insert into the membrane to aid in channel formation⁵⁸. Regulation of CLIC1s membrane bound form via redox signalling has been suggested due to the existence of a glutaredoxin-like active site⁵⁸. More recent literature has shown that increasing concentrations of cations such as zinc (Zn^{2+}) and calcium (Ca^{2+}) triggers CLIC1 insertion into the membrane when reconstituted in synthetic phospholipid vesicles. This data strongly suggests that CLIC1 therefore contains a cation binding site⁶⁴. Moreover, calcium Ca^{2+} binding sites have been located in two invertebrate homologues of CLIC1, EXC-4 and DmCLIC⁶⁷. The calcium binding site overlaps the GSH binding site found in GSTs. This has all led to the hypothesis that cation binding to CLIC1 causes a conformational shift that releases the putative transmembrane domain allowing it to help assist in membrane insertions. CLIC1 is also implicated in many cancers such as glioblastoma⁶⁸, lung adenocarcinoma^{69,70}, hepatocarcinoma⁷⁰ and gastric carcinoma⁷¹.

8.9 Project Aims:

The aim of this project is to better understand the soluble structure and enzymatic activity of the proteins GSTO1 and CLIC1 and to compare and contrast these homologues. Both already have well-defined structures as they have been extensively studied using X-ray crystallography as evidenced by the many crystal structures in the Protein Data Bank. However, the structure of a protein in a crystal can be different to that of the same protein in solute. When crystalised the proteins' structure is completely static, for that reason further structural analysis of GSTO1 and CLIC1 using other techniques such as Small Angle X-ray Scattering and Nuclear Magnetic Resonance can help elucidate more information about the protein, as they show the proteins structure in solute allowing the protein to be in a dynamic state. This is important to know as this dynamic state is how GSTO1 and CLIC would look in vivo. Furthermore, the NMR can be used to study the proteins dynamics which cannot be inferred from a typical crystal structure or many other forms of experiments. This can help us better understand the enzymatic activity of the proteins which is not as well understood as its structure. Various computational techniques will also be used to compliment the experimental data. As it is known that CLIC1 inserts into the membrane and GSTO1 does not, any differences found in the structure may help better understand the differences that must exist allowing CLIC1 to insert into the membrane. This is where a current gap in the literature lies, and these experiments aim to help understand this gap.

9 Materials and Methods

9.1 Transformations:

1 μ l of DNA was added to 10 μ l of C43 cells and mixed with the pipette tip, then incubated on ice for 15 mins. The mixture was then heat shocked at 42°C for 45 seconds, then transferred immediately to ice for 5 minutes. 500 ml of Lb was added to the mixture then transferred into a shaking incubator where it was left for 1 hour at 37°C. 250 ml of the mixture was then transferred onto an agar plate with a ratio of 1/1000 antibiotic/LB.

9.2 Cell Growth:

GSTO1 and CLIC1 were both grown using ampicillin (AMP). A starter was made by inoculating 50 ml of LB in a 200 ml conical flask with a colony from the transformation plate. The starter was left to grow overnight at 37°C with AMP (1 ml/L). The starter was added to 1 L of LB and grown to an OD of 0.7 at 37°C in AMP (1 ml/L) in 2 L plastic conical flasks. Once an OD of 0.7 was reached 1 ml of IPTG (1 ml/L) was added and left to grow in a shaking incubator at 30°C overnight. The cells were then poured from the growth flasks into centrifuge bottles and balanced within 0.1 g of each other. The cells were then spun down at 6000rpm for 15 minutes at 4°C. The cells were always kept on ice when not being spun down. The supernatant was poured away immediately after the cells had been spun down, and the pellets resuspended in 100 ml lysis buffer. Finally, protease inhibitor was added to the cells and flash frozen in liquid nitrogen for storage.

9.3 Protein Purification:

Lysis buffer – 50 mM Tris, 150 mM NaCl, 1 mM DTT, pH 8

Wash buffer – Same as lysis buffer

Elution buffer – Same as lysis buffer + 500 mM imidazole

Dialysis buffer – 20 mM Tris, 150 mM NaCl and 1.5 mM CaCl₂, pH 8

The cells were thawed out and sonicated for 15 seconds on 15 seconds off for a total time of 20 minutes, the solution went from light brown to dark brown. The sonicated cells are then placed in ultracentrifuge tubes and balanced to exactly 0.0 g difference. The cells were then spun down at 45,000 rpm for 45 minutes at 4°C, once finished the supernatant was poured into a falcon tube and kept on ice as the sample. Next the supernatant was run through a nickel gravity column. To prepare the column it was first left to drain then 20ml water was run through and finally 20 ml lysis buffer was run through. The sample (supernatant) was run through the column and flowthrough collected in 50 ml falcon tubes. Next 20 ml of wash buffer was run through (the first 5 ml was collected as flowthrough) then the rest collected as wash. Finally, 20 ml elution buffer was run through and collected as elution. To store the column 20 ml of water was run through then the column was stored in 20% ethanol. A SDS page gel was run using the column samples to see where and if the protein eluted. The protein was then transferred into a dialysis membrane and (1 U/ml) of thrombin was added. The protein in the membrane was then added to 5L of dialysis buffer at 4°C and left overnight. The cleaved protein was then transferred from the dialysis bag into a falcon tube and kept on ice. Next a reverse nickel column was run using the cleaved protein. This

means the flowthrough was collected as the sample as it contains the cleaved protein. The column was run using the same method as day 1. Another gel was run to make sure the protein was cleaved and eluted in the flowthrough. The cleaved protein, now with a continuing a gh sequence and referred to as 'wild type' in the Thermofluor experiments, was then concentrated down to ~10 mg/ml using spin concentrators at 4000 rpm at 4°C for 10 mins. The sample was then flash frozen in liquid nitrogen. The protein was thawed out and then run through a SEC column.

9.4 Multiple sequence alignment:

The sequences of GSTO1 and CLIC1 were aligned using Clustal Omega with default settings⁷².

9.5 Structural alignment:

The structural alignment of GSTO1 and CLIC1 was carried out using their crystal structures 1eem and 1k0m respectively. The alignment was performed using PyMOL's align function⁷³. Monomer A was deleted in CLIC1 along with all the water molecules. Glu-63 in monomer B of 1k0m was mutated using PyMOL's mutagenesis function into Gln-63, and rotamer 4 was chosen as it had the least atom clashes. This was done as the crystal structure sequence does not match to the uniport sequence.

9.6 SAXS:

SAXS samples were collected on Beamline 21 in the synchrotron at Diamond light source. GSTO1 samples existed between 10-20 mg/ml and were in 20 mM NaCl, 20 mM phosphate 5% glycerol pH 7.4. While CLIC1 samples existed between 10-20 mg/ml and were in 50 mM Hepes buffer pH 7.4 with 5% glycerol. SEC-SAXS was implemented, and the SEC column coupled with the SAXS was the KW-403 Shodex. The results were analysed using SCATTER and fitted to the crystal structures using FoXES web server.

9.7 B Factor analysis:

B factors from GSTO1 (PBD ID:1eem) and CLIC1 (PBD ID:1k0m) were calculated using Disulphide by Design v2.13 on default settings⁷⁴. The individual B-factors for each residue and a mean B-factor for the whole protein is displayed. The B Factors for each residue were then plotted on a graph in Excel. Using PyMOL's B Factor putty function a visual representation was generated of both GSTO1 (PBD ID:1eem) and CLIC1 (PBD ID:1k0m).

9.8 Intramolecular bond analysis:

To compare the amount and type of bonds between GSTO1 (PBD ID:1eem) and CLIC1 (PBD ID:1k0m) C and N-domains, and the loops that connects them Protein Interaction Calculator (PIC interactions) was used⁷⁵. The crystal structures were uploaded in PBD format and run on default settings with all intramolecular interactions selected. These were then counted and put into tables. As 1k0m contains monomer A and B duplicate interactions from monomer A were not counted.

9.9 Thermofluor analysis:

The Thermofluor samples were prepared by adding 2.5 μL of protein from a 100 μM stock, 10 μL of sypro dye from a 500x stock and 37.5 μL of reaction buffer to each well for a total volume of 50 μL . Samples were pipetted into a clear 96 well thin-wall PCR plate and the plate sealed with optically clear adhesive sheets. The Thermofluor assay was carried out using an Applied Biosystems QuantStudio 5 Real-Time PCR System. Using the ROX dye calibrations the detector, setting the passive reference at none and excitation at 485 nm and emission at 570 nm. The temperature ramp was set to increase 1.5°C every 2 minutes from 25°C to 99°C. Results were analysed using the QuantStudio 5 software.

9.10 NMR:

GSTO1 NMR samples were concentrated down to 100-250 μM in 20 mM NaCl 20 mM Phosphate pH 7.4. CLIC1 NMR samples were concentrated down to 100-200 μM in HEPES NMR buffer pH 7.4 and collected at 30°C on a Bruker spectrometer which operates at a ^1H frequency of 600MHz. Samples were collected at 300 μL with 15 μL /5% D_2O added in shigemi tubes. For GSTO1 a BTROSY-HSQC experiment was run and for CLIC1 a SOFAST-HMQC experiment was run.

9.11 PEPTIDE SYNTHESIS AND PURIFICATION:

The peptide (SQLWCLSN) 1076.3 Daltons was dissolved in 0.1 M ammonium acetate, pH 8.0, and glutathionylated by incubating with a 10-fold molar excess of oxidized glutathione for

24 h at room temperature with constant stirring. Next a HPLC was used to purify the saturated protein from the mix. This pure fraction of saturated protein was then lyophilized using a vacuum pump then it could be redissolved as needed into the NMR sample.

10 Results

The aim of this project is to better understand both the structure and enzymatic activity of both GSTO1 and CLIC1. By using a variety of methods both computational and experimental to try and uncover the differences between the two homologues crystal structures, as well as the difference between their crystal structure and their structures in solution. In the hope that the differences discovered may help explain how CLIC1 can insert into the membrane.

Chapter 1

10.1 Sequence and structural alignments of GSTO1 and CLIC1:

GSTO1 and CLIC1 have long been known to be structural homologues and both having the ability to bind GSH. When CLIC1 adopts its soluble form, it assumes the same folds as a GST protein. A multiple sequence alignment using Clustal Omega was carried out as shown in figure 4. The alignment shows a high amount of conservation with 46 amino acids being fully conserved, 42 amino acids having conservation between amino acids of strongly similar properties and 27 amino acids having conservation between amino acids of weakly similar properties. This is consistent with GSTO1 and CLIC1 being structural homologues.

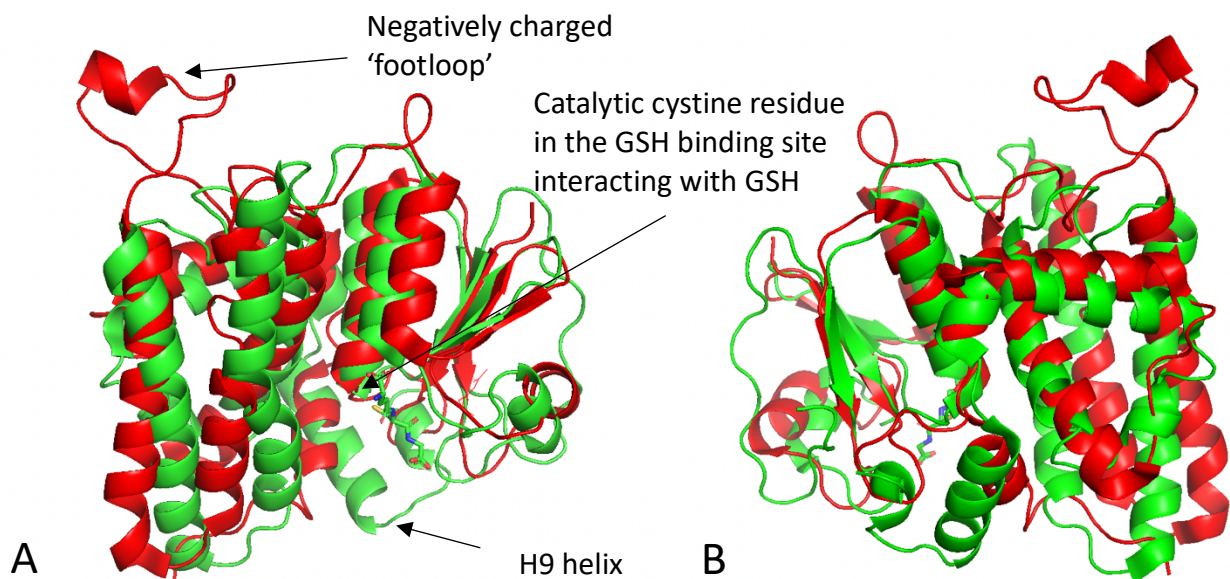


Figure 6: A structural alignment of GSTO1 and CLIC1.

A) Shows GSTO1 (PBD ID:1eem) shown in green and CLIC1 (PBD ID:1k0m) shown in red. This alignment shows a high homology between the two structures. However, some clear differences can be noted such as CLIC1 negatively charged 'footloop' which is absent in GSTO1, and the positioning of the H9 helix. Both of which are labeled in the figure above. The catalytic cystine residue found in the GSH binding site is also shown, C32 for GSTO1 and C24 for CLIC1. B) Shows the same alignment rotated 180°.

Whilst the structural homology is high there are some notable differences, these included CLIC1's negatively charged 'footloop' found between the helices H5 and H6. This loop while not thought to have a role in binding is highly negatively charged containing 7 acidic residues. It is also located spatially next to the loop linking CLICs two domains. This could suggest a role in any conformational change. Another notable difference is that of the positioning of the helix H9 which in GST forms the 'lid' of the H binding site. This H site in CLIC1 is more elongated and open than in GSTO1, as can be seen in the figure above.

10.2 Elucidating the in-Solution Structures and Conformational Dynamics of GSTO1 and CLIC1 using SAXS:

As well as the computational sequence and structural alignment experimental SAXS data was collected on both GSTO1 and CLIC1. Figure 7 A) shows a plot of the experimental SAXS curve for GSTO1 shown in black, and the theoretical SAXS curve derived from the X-ray crystal structure of GSTO1 (PDB ID: 1eem <http://www.rcsb.org/pdb/explore.do?structureId=1Z7E>) shown in red. Figure 7 B) shows a plot of the experimental SAXS curve for CLIC1 shown in black, and the theoretical SAXS curve derived from the X-ray crystal structure of CLIC1 (PDB ID: 1k0m <http://www.rcsb.org/pdb/explore.do?structureId=1Z7E>).

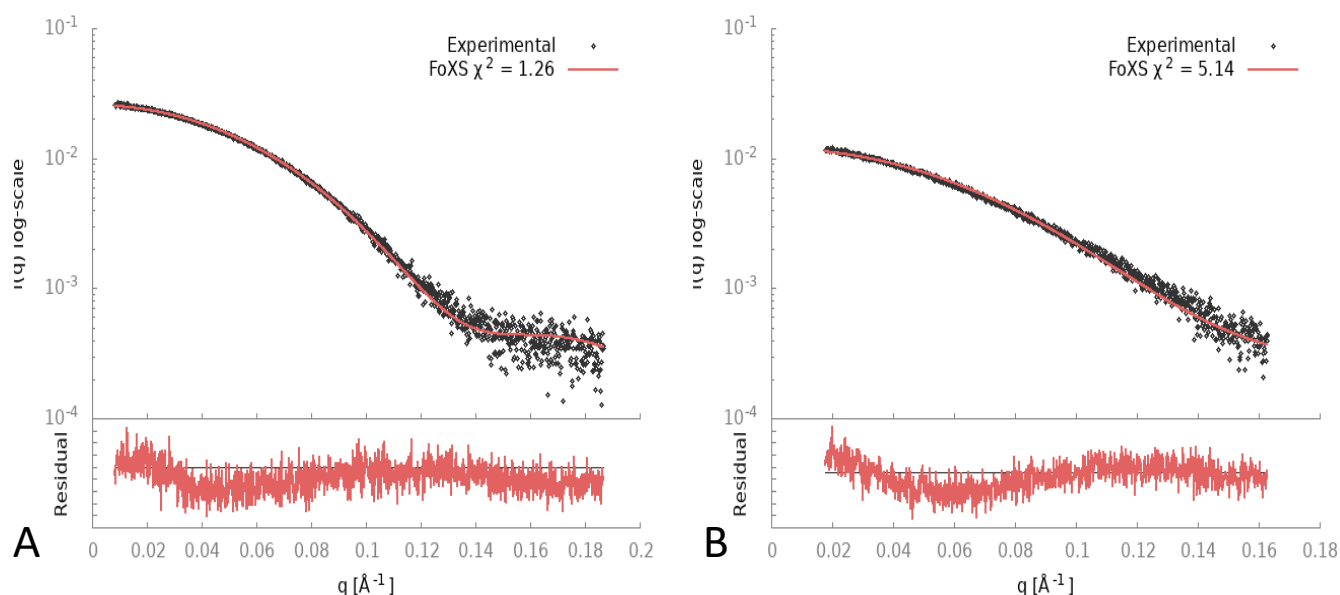


Figure 7: A graph showing experimental scattering data plotted against the theoretical SAXS curve of the crystal structure.

A) Shows the theoretical scattering curve of GSTO1 crystal structure (PDB ID: 1eem) in red against the experimental scattering data of GSTO1 shown in black. Also shown is the Chi squared of the fit between the two. B) Shows the theoretical scattering curve of CLIC1 crystal structure (PDB ID: 1k0m) in red against the experimental scattering data of CLIC1 in black. Also shown is the Chi squared of the fit between the two.

The chi squared for the fit of the scattering data to the crystal structure for A and B is calculated and shown in figure 7 above. A chi squared score of 1 is seen as ideal for SAXS data as anything below this likely means you are overfitting the data or the error estimates are too large. Therefore (A) chi squared value of 1.26 means this data is a very good fit to the x-ray crystal structure and the x-ray structure is likely to be what we would see in solution. (B) shows a chi squared value of 5.14, this is a high chi squared score therefore the fit of the data is not good and the crystal structure is likely to be not what we would see in solution.

The $P(r)$ is a distance distribution function and can be obtained via an indirect Fourier transformation of the scattering data, and is used to determine the shape of a protein's envelope. Using the experimental data gathered two $P(r)$ were created as shown in figure 8.

Figure 8 A) shows the $P(r)$ plot of GSTO1 and B) shows the $P(r)$ plot of CLIC1.

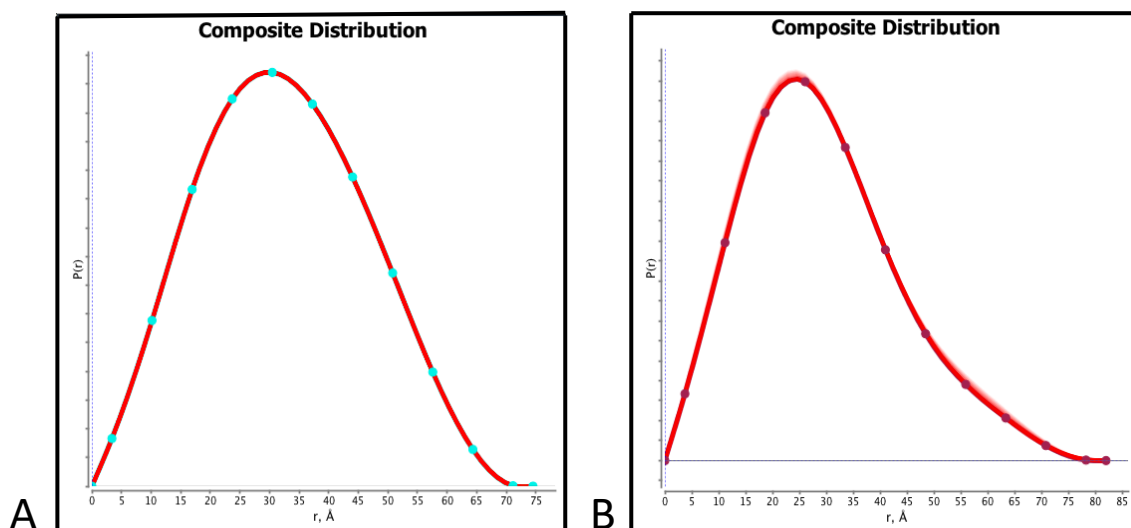


Figure 8: $P(r)$ graphs for GSTO1 and CLIC1.
A) Shows a $P(r)$ graph of GSTO1. B) Shows the $P(r)$ plot for CLIC1

The symmetrical bell-shaped curve on the $P(r)$ plot shown figure 8 (A) would indicate that GSTO1 is a globular protein. This would support the close fit of the experimental scattering SAXS to that of the compact globular crystal structures of GSTO1. Interestingly CLIC1's $P(r)$ plot as shown in figure 8 (B) is not a symmetrical bell-shaped curve and instead has a 'tail'. This would imply a certain amount of disorder in the protein and it not being as compact and globular. The difference in shape of the $P(r)$ plot, along with the high chi squared value in figure 7 (B), would suggest that the in-solution structure for CLIC1 and GSTO1 are not as similar as their crystal structure. This could help explain why the supposed homologues have very different functions in vivo.

10.3 Measuring protein flexibility, subunit-subunit interactions and intramolecular dynamics for GSTO1 and CLIC1:

To further probe the potential difference of the structure in solution some further analysis was carried out using B factors. Simplified a B factor is the precision of an atoms position in a crystal structure. The uncertainty can be due to disorder in the crystal when the measurement was taken. B factors can therefore be used to indicate the flexibility of parts of a protein. Shown below in figures 9 and 10 are the B factors for every amino acid in GSTO1 and CLIC1. Stretches of amino acids with high B factors may indicate areas of the protein functionally important to flexibility and therefore conformational change.

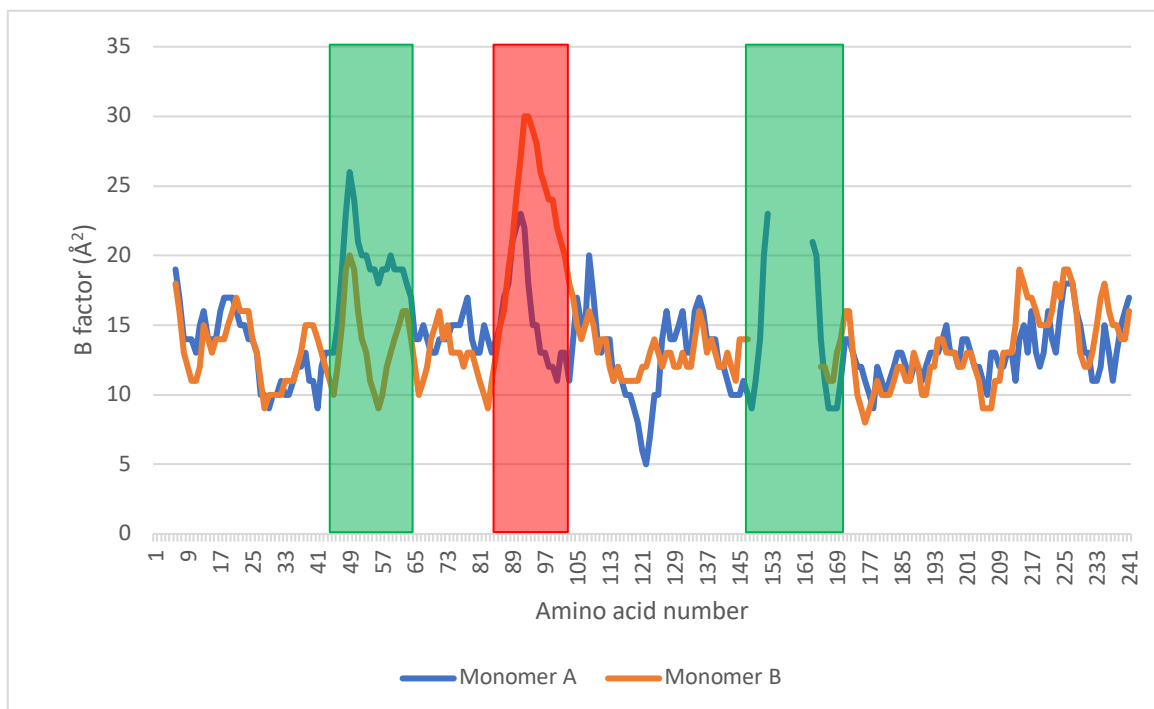


Figure 9: A graph plotting all B factors for each amino acid in CLIC1's (PBD ID: 1k0m) monomer A and B.

B factors for monomer A are shown in blue and for B are shown in orange. Regions of significantly higher B factors are highlighted in green. The loop connecting the C and N-domains of CLIC1 is also highlighted in red (residues 88-100). The mean B-factor of 1k0m is 10.152\AA^2 as shown by the back dotted line.

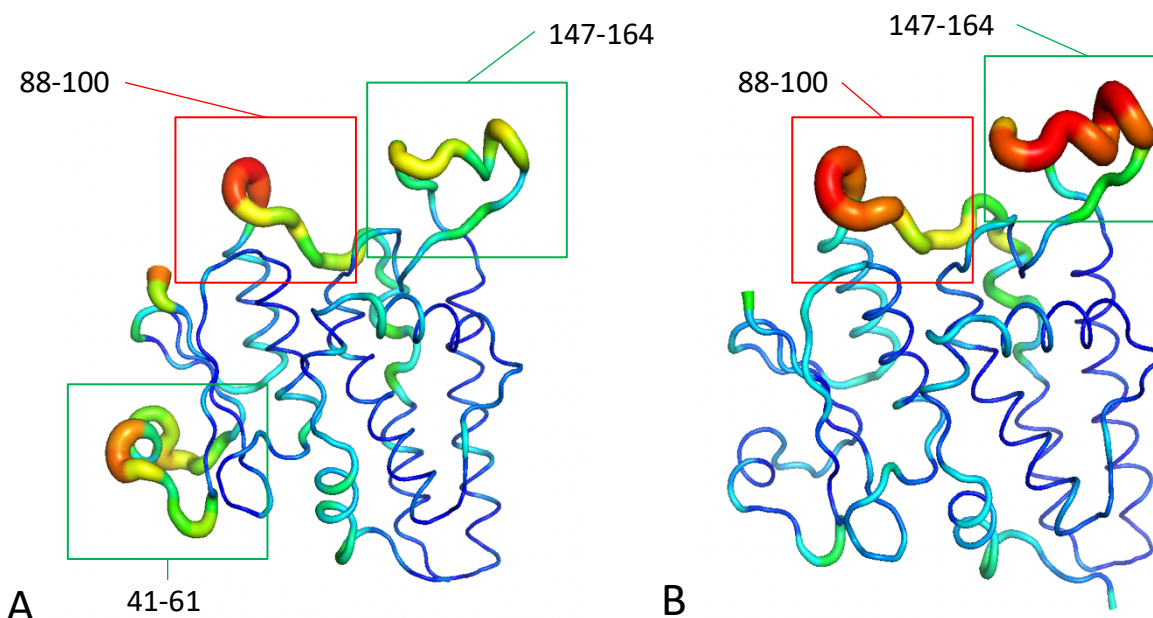


Figure 10: B factor visually displayed on CLIC1's crystal structure (PBD ID: 1k0m).

A) Shows the B factor of each residue in monomer A of CLIC1 represented by thickness of the backbone (the thicker the backbone the higher the B factor) and colour (red indicates a high B factor and blue represents a low B factor.) B) shows the same for monomer B of CLIC1. Highlighted by a red box in both A) and B) is the loop connecting the C and N-terminus, green boxes highlight other areas of high B factor also highlighted in figure 9.

Figure 9 shows the monomers A and B of CLIC1's and the B factor for each residue. Areas of notably higher than average B factor have been highlighted. Highlighted in red is 88-100 which is the loop connecting the C and N terminus, with the loop of monomer A having a slightly lower B factor than that of monomer B. This is further visualised in figure 10 showing the B factors on the crystal structure. The high B factor would indicate the area is likely flexible and could be involved in the protein's dynamics. The 'foot loop' region of monomer B also has a B factor significantly higher than the average however, interestingly this is not the case for monomer A. The inverse is true for loop between residues 41-61 with the B factor being higher than average for monomer A but not monomer B.

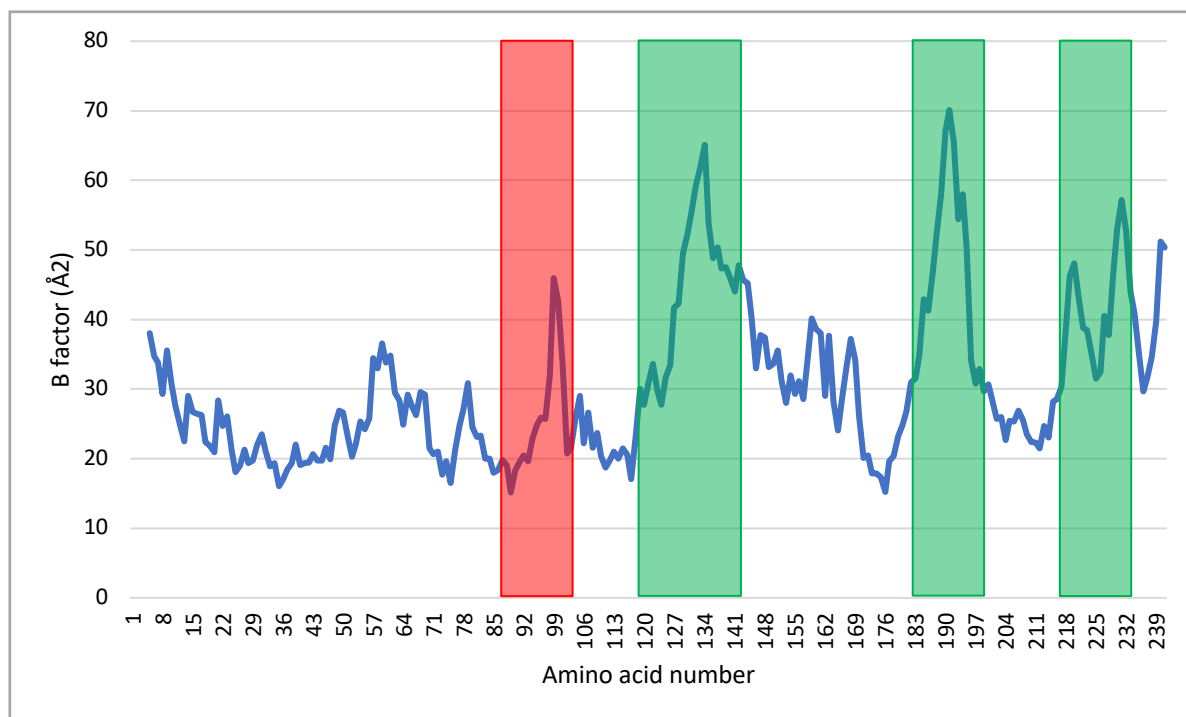


Figure 11: A graph plotting the B factor for each amino acid in GSTO1 (PDB ID: 1eem). Regions of significantly higher B factor are highlighted in green. The loop connecting the C and N-terminus is highlighted in red. The mean B factor of 1eem is 30.704 \AA^2 as shown by the black dotted line.

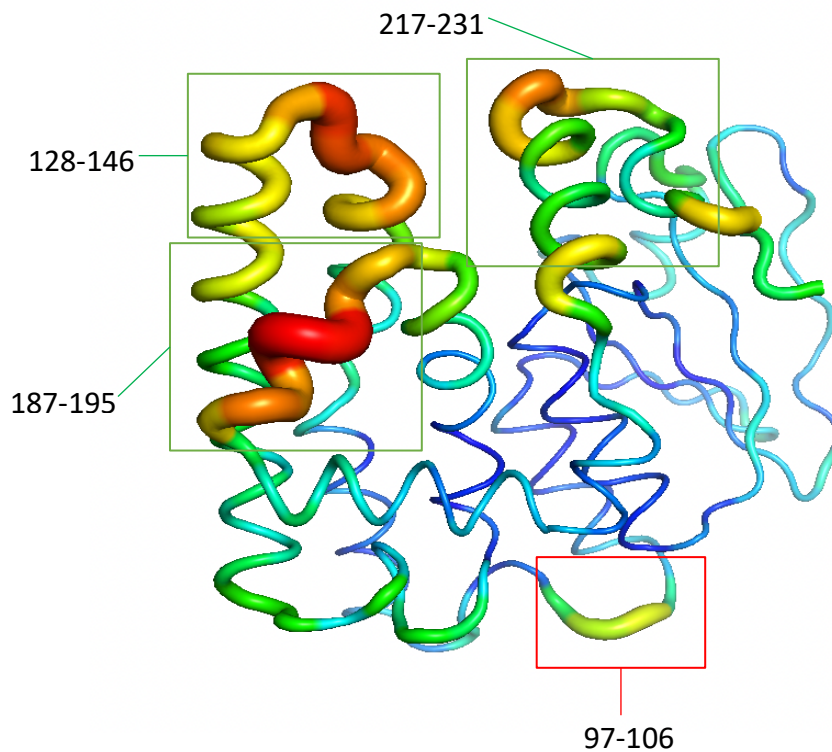


Figure 12: B factor visually displayed on GSTO1's crystal structure (PDB ID: 1eem). The B factor of each residue is represented by the thickness of the backbone (the thicker the backbone the higher the B factor) and colour (red indicates a high B factor and blue represents a low B factor). Areas of above average B factor are highlighted in green boxes and the loop linking the C and N-terminus is highlighted in a red box.

GSTO1's average B factor is higher than that of CLIC1's as can be seen in figures 8 and 10 however; this is likely due to the lower resolution crystal structure of GSTO1 (2.40Å) in comparison to CLIC1's crystal structure (1.40Å). The areas with the highest B factor in GSTO1 are highlighted in green in figure 11 and 12, these areas are not found to have a high B factor in CLIC1. The loop linking the N and C-domains of GSTO1 highlighted in red (97-106) has a lower average B factor than the same linking loop in CLIC1. Only two of the residues in this loop, 99 and 100 have a higher-than-average B factor for GSTO1. The low average B factor in residues 97-106 in GSTO1 would indicate it is not especially flexible and therefore unlikely to assist in any major conformational change. The opposite however could be said

for the loop linking CLIC1s C and N-domains with the high B factor and pivotal location making it a potential candidate to explain the different shape CLIC1 adopts in solution.

NMR spin relaxation experiment for CLIC1:

While B factors can be useful in finding potentially flexible areas of a protein it is limited in scope. Some of these limitations are it is only computational, it is based on the crystal structure and the rate of exchange is not known, this means the timescale of the movement is impossible to derive. Therefore, the difference between disorder and a slow conformational shift cannot be determined. For this reason, an NMR spin relaxation experiment was performed. By measuring the R1 (fast backbone movements picosecond to nanosecond (ps-ns) timescale) and R2 (slower backbone dynamics in the microsecond to millisecond (μ s-ms) timescale) a R2/R1 ratio could be used to tell which residues had fast motions and which had slow. Above the R2/R1 mean of the proteins indicates slow motions potentially related to function whereas, areas below this average correlates to fast motions related to disorder. This can be seen in figure 13 below.

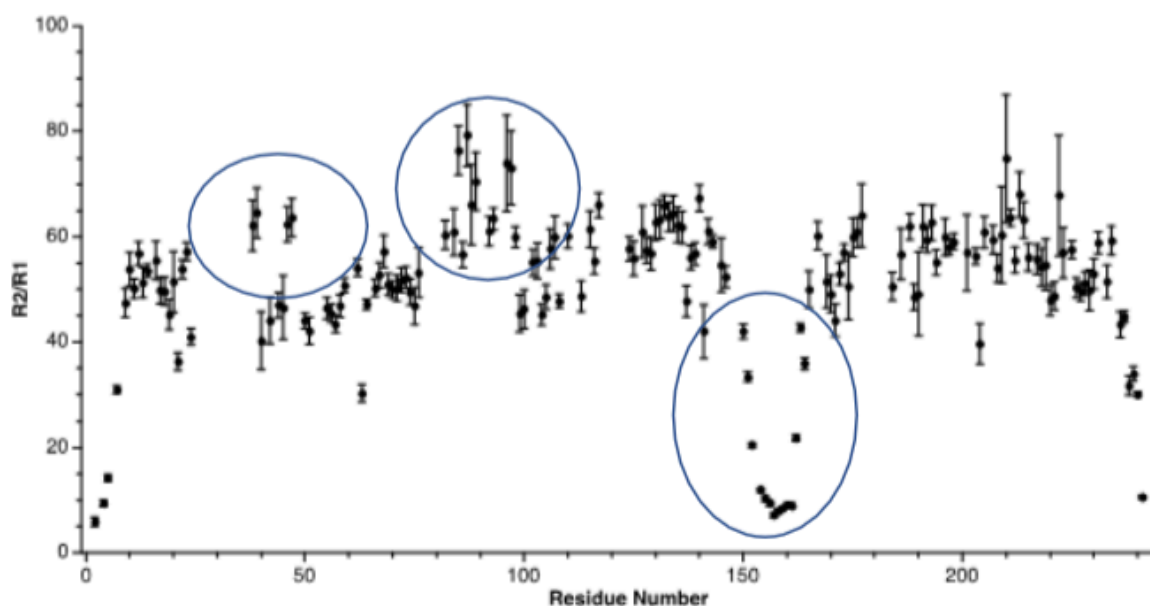


Figure 13: NMR spin relaxation of CLIC1.

^{15}N R_2/R_1 values of 250mM CLIC1 in PBS buffer, pH 7.4 plotted against their residue number. Areas above or below the mean R_2/R_1 ratio of the protein are highlighted in blue. The data was taken from Dr Jose Ortega-Roldan's lab.

All the areas highlighted in blue above in figure 13 were also areas of interest in the B factor analyse, figures 8-11. Residues 40-50 are highlighted in figure 9 as residues 41-61 in figure 10, the data in figure 13 shows experimentally in solution that this area does indeed move and that it is an area of slow movement as the R_2/R_1 values are above that of the average for the protein. Meaning it is potentially involved in a conformational shift. Residues 145-165 are below the R_2/R_1 average value making it an area of fast movement, most likely disorder of the backbone. Therefore, this area of the protein is less likely to be involved in any large conformational shifts. Finally, residues 88-100 are shown as having an above average R_2/R_1 ratio. This would line up with the B factor analysis predicting the flexibility and show this area does exhibit slow movement. The fact this area does not have high

predicted flexibility in GSTO1 as well as its prime location linking the C and N-domains makes it a likely candidate for the difference in SAXS structure between GSTO1 and CLIC1

Intramolecular non-covalent bond and interactions analysis:

With the hypothesis that the loop between the N and C-terminus is facilitating a potential conformational shift in CLIC1 but not in GSTO1 some further analysis was done to see if this could be the case. An analysis on the amount and type of intramolecular non-covalent bonds between the N and C-domains of CLIC1 in comparison GSTO1 was carried out in order to shed some light on this.

Table 1: Intramolecular non-covalent bonds and interactions predicted in CLIC1 crystal structure (PBD:1k0m).

Below shows predicted interaction in areas of interest of CLIC1 with focus on the interface between the N and C-domains.

| CLIC1 | Hydrophobic interactions | Main chain- Main chain hydrogen bonds | Main chain- Side chain hydrogen bons | Side chain- Side chain hydrogen bonds | Cation Pi interactions | Ionic interactions | Total |
|---|--------------------------|--|---|--|---------------------------|-----------------------|-------|
| Across the N and C- domain interface | 9 | 0 | 7 | 11 | 1 | 2 | 30 |
| N-domain to linker | 8 | 2 | 6 | 0 | 0 | 1 | 17 |
| C-domain to linker | 3 | 3 | 4 | 4 | 0 | 0 | 14 |
| Total | 20 | 5 | 17 | 15 | 1 | 3 | 61 |

Table 2: Intramolecular non-covalent bonds and interactions predicted in GSTO1 crystal structure (PBD:1eem).

Below shows predicted interaction in areas of interest of GSTO1 with focus on the interface between the N and C-domains.

| GSTO1 | Hydrophobic interactions | Main chain- Main chain hydrogen bonds | Main chain- Side chain hydrogen bonds | Side chain- Side chain hydrogen bonds | Cation Pi interactions | Ionic interactions | Aromatic- Aromatic interactions | Aromatic- Sulphur interactions | Total |
|-------------------------------------|--------------------------|---|---|---|------------------------|--------------------|------------------------------------|-----------------------------------|-------|
| Across the N and C-domain interface | 20 | 0 | 16 | 15 | 2 | 4 | 2 | 1 | 60 |
| N-domain to linker | 7 | 1 | 4 | 4 | 0 | 1 | 1 | 0 | 18 |
| C-domain to linker | 4 | 4 | 4 | 4 | 0 | 1 | 0 | 0 | 17 |
| Total | 31 | 5 | 24 | 23 | 2 | 6 | 3 | 1 | 95 |

As shown above in tables 1 and 2 GSTO1 has double the total amount of intramolecular non-covalent bonds between subunits than CLIC1 has. This includes 20 hydrophobic interactions to CLIC1s 9, 15 main chain-side chain hydrogen bonds to CLIC1s 7 and 4 ionic interactions to CLIC1s 2. GSTO1 also has aromatic-sulphur and aromatic-aromatic interactions that are not predicted in CLIC1. The higher number of interactions between the domains in GSTO1 does fit with the hypothesis that GSTO1 is globular and has minimal movement between domains whereas, CLIC1s 88-100 loop is facilitating a conformational shift between the domains.

Thermofluor analysis:

The fewer intramolecular non-covalent bonds and interactions between the two domains of CLIC1 in comparison to GSTO1 as shown in the tables above, as well as the less globular shape suggested by the SAXS data should mean that CLIC1 will denature at a lower temperature than GSTO1. To test this, we measured the T_m or melting point of both proteins. A thermofluor stability assay using sypro orange dye was used to measure the T_m . Sypro orange is a dye that exhibits fluorescence when it binds to hydrophobic surfaces. Using a QPCR machine the protein is slowly heated up until denatured. As the protein unfolds the dye starts to bind to the hydrophobic areas that are becoming unravelled, and the fluorescence increase is measured by the QPCR. The T_m can be extrapolated when the fluorescence reaches its peak. Below are the melt curves of both CLIC1 and GSTO1.

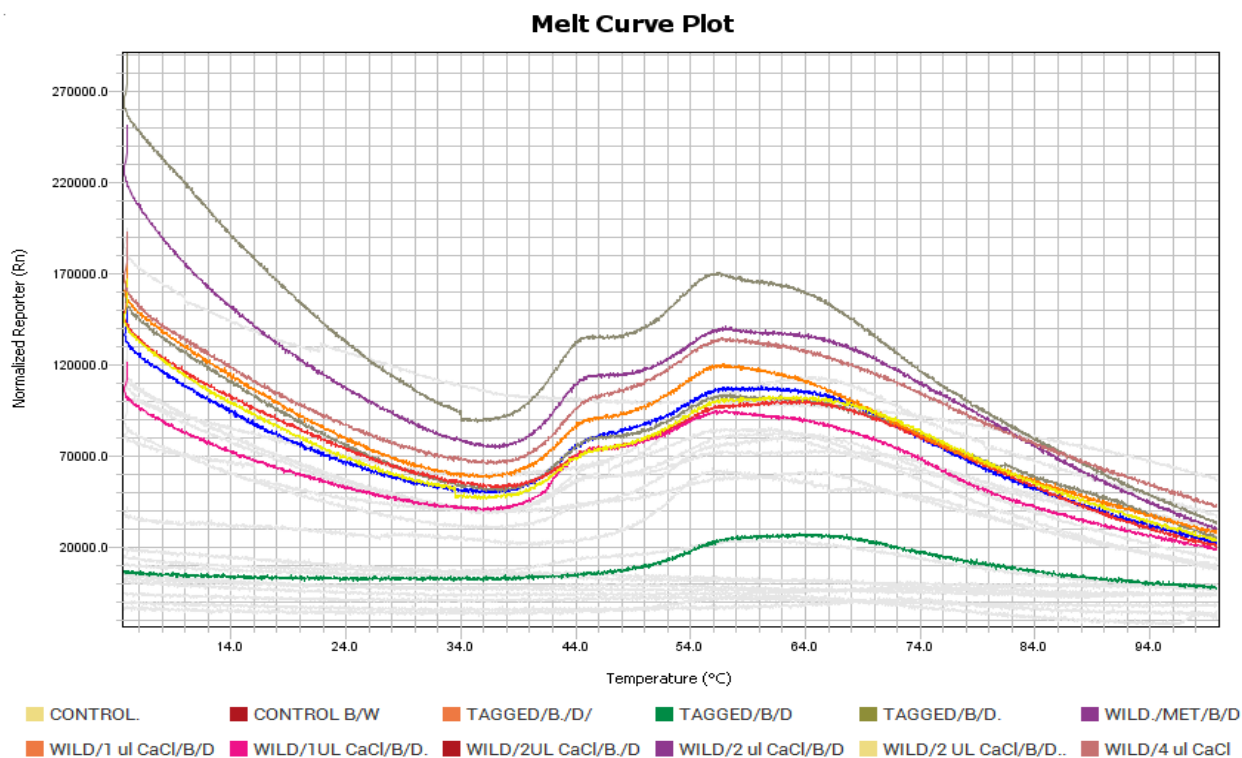


Figure 14: Shows the Thermofluor melt curve plot for soluble wild type CLIC1 and un-cleaved His-tagged CLIC1.

Un-cleaved and wild type CLIC1 are indicated by colour code.

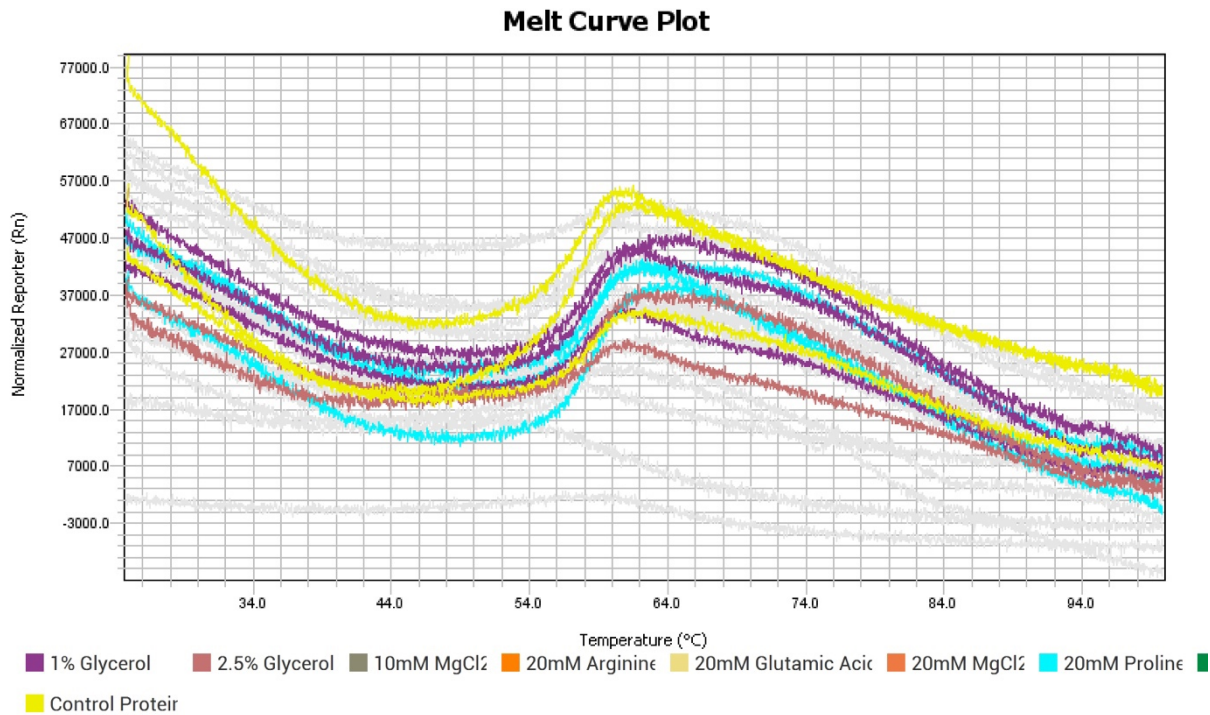


Figure 15: Shows the ThermoFluor melt curve plot for GSTO1 in various buffers. Individual buffers for GSTO1 are indicated by colour code.

As shown above in figures 13 and 14 GSTO1 has a T_m of between 60-62°C whereas CLIC1 has a T_m of 56-58°C. Such a large difference in T_m as well as the rest of the data we have gathered such as the fewer number and type of intramolecular interactions shown in tables 1 and 2, the less globular shape the SAXS data predicts in figures 1 and 2, and finally the evidence of slow movement indicative of function gathered from the CLIC1 NMR spin relaxation experiment. These all point towards the theory that the crystal structure for CLIC1 with the extremely high homology for GSTO1 is incorrect and is not the conformation CLIC1 adopts in solution. Another point of interest in figure 15 is the double transition CLIC1 goes through while denaturing and the fact it does not go through this transition when the His-tag is left un-cleaved.

Chapter 2:

The next step after analysing CLIC1 and GSTO1 structural homology was to compare the protein dynamics of both while binding to a ligand. GSH is a ligand both GSTO1 and CLIC1 bind with and therefore was used for comparison.

10.4 Comparison of the GSH binding site on GSTO1 and CLIC1:

Solution NMR can be used to determine the regions affected by binding in proteins.

To observe the interaction between GSTO1 and GSH a titration monitored by NMR was carried out. A BEST TROSY HSQC NMR experiment was collected in the absence and presence of GSH. A TROSY HSQC experiment was chosen as GSTO1 in solution is a relatively large molecule for NMR at a 55kD dimer, and as shown above very globular. These two factors result in GSTO1 'tumbling' slowly in solution therefore, to obtain the best results a TROSY HSQC was the most suitable NMR experiment. Using a ^{15}N -labelled sample of GSTO1 and starting at a molar ratio of 0 GSH the spectrum was recorded. After each run the molar ratio of GSTO1 to GSH was increased by 0.25 until a molar ratio of 2 was reached. This was when we deemed when the GSTO1 was most likely fully saturated as no further shift of the backbone resonance was observed. The titrations can be seen below in figure 16.

GSTO1 titration with glutathione (GSH)

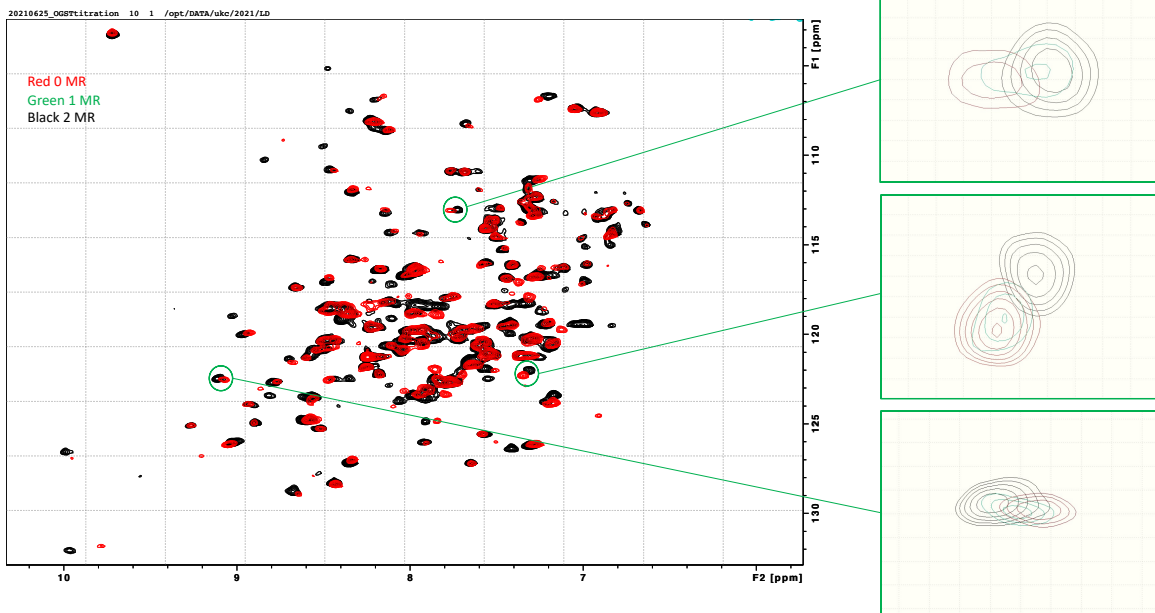


Figure 16: BEST TROSY HSQC spectra of GSTO1 at 181uM, 308K, pH 7.4, 20mM NaCl, 20mM Phosphate.

Three spectra aligned and overlaid with each other. A 0 molar ratio of GSH in red, a 1 molar ratio in green and a 2 molar ratio in black.

Figure 16 above shows three BEST TROSY HSQC experiments overlaid, with GSH at a molar ratio of 0, 1 and 2. As evidenced by the magnified peaks highlighted in the green boxes there is a clear chemical shift when GSH is titrated into the sample, meaning GSTO1 is binding to GSH, and this is causing changes in the chemical environment around a subset of peaks in the protein. Unfortunately, we are unable to determine the residue number of the peaks that are shifting as the assignment of GSTO1 could not be completed due to the data not being of high enough quality.

To observe the structural shifts of CLIC1 binding GSH the same titration was carried out.

However, this time a SOFAST HMQC NMR experiment was run instead of a TROSY HSQC due to its increase sensitivity and a molar ratio of 3 was reached. The results of this can be seen in figure 17 below.

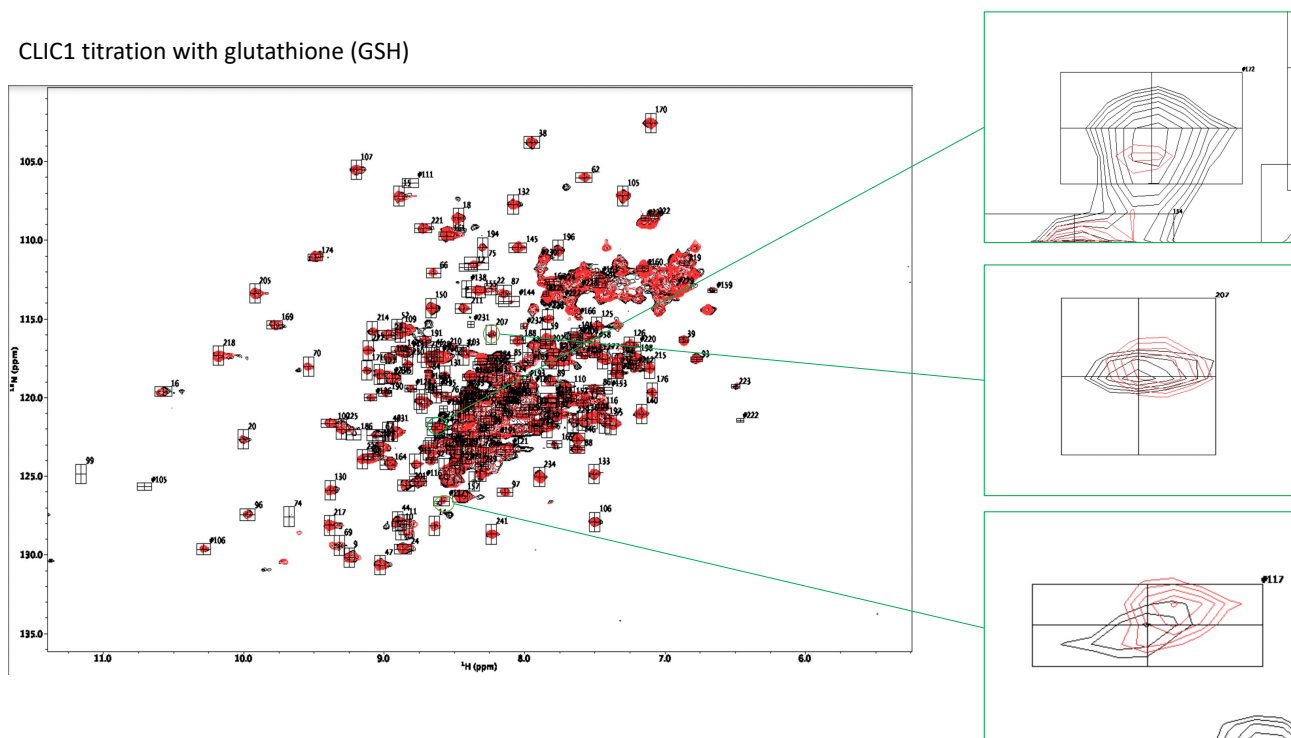


Figure 17: SOFAST spectrums of CLIC1 at 181uM, 308K, pH 7.4, 20mM NaCl, Phosphate 20mM.

Two spectrums aligned and overlaid with each other. A 0 molar ratio of GSH in red and a 3 molar ratio in black.

Figure 17 above shows three SOFAST experiments overlaid, with GSH at a molar ratio of 0 and 3. As can be seen in figure 17 above there is less shifting of residues in this titration and more of residues changing in intensity Unlike GSTO1 we do have assignments for CLIC1 meaning we can assign each chemical shift on the spectrum to a residue in the backbone and therefore identify exactly which residues and therefore areas of the protein are undergoing a conformational change. This is visualised in figure 18 below showing the

chemical shift in ppm for each residue in CLIC1 when bound to GSH. In figure 18 the most shifted residue is V74 which shifted 0.177ppm, this is significantly above the mean shift for the assigned residues of 0.004ppm indicated by the yellow line in figure 18 below. V74 is further visualised in figure 19 in red and can be seen to sit in the binding pocket. Residue F69 is the next most shifted residue 0.04ppm.

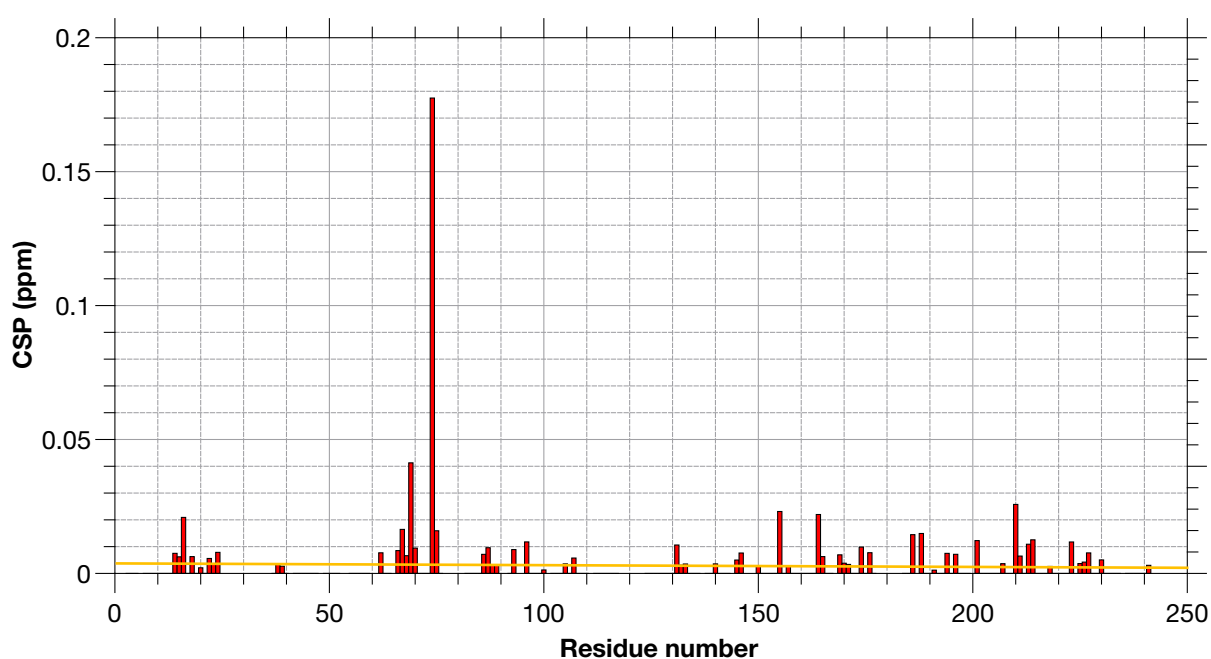


Figure 18: Chemical shifts (ppm) plotted against amino acid number for CLIC1. A graph showing the chemical shift in ppm for each residue in CLIC1 after GSH was added to the solution. The yellow line indicates the mean chemical shift for assigned residues (0.004ppm).

The chemical shifts from figure 18 were then visualised on the CLIC1s x-ray crystal structure (PBD:1k0m) as shown in figure 19 below

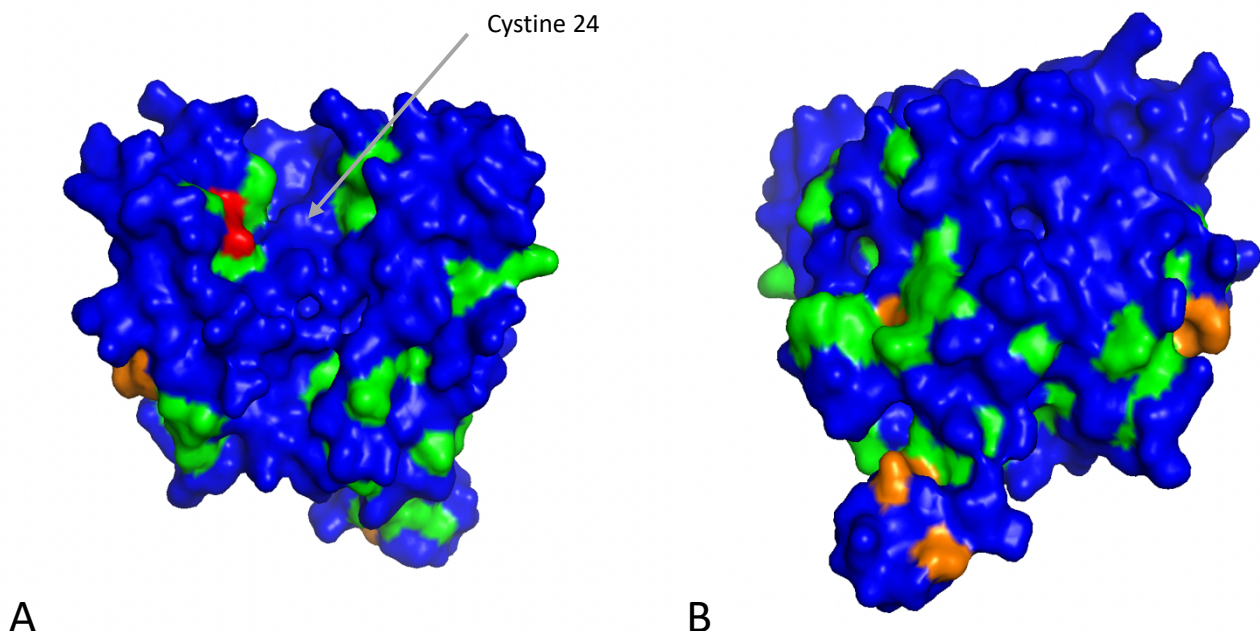


Figure 19: A visual representation of chemical shift in CLIC1's (PBD:1k0m) amino acids when binding to GSH.

A) Shows chemical shifts (ppm) greater than 0.05 are shown in red, 0.02 in orange, 0.00 in green and areas of 0 chemical shift are shown in blue. The grey arrow points to the cystine 24 which binds GSH. B) shows the same model but rotated 180.

Residues that shifted greater than 0.05 ppm are shown in red, 0.02 in orange and 0.00 in green. CLIC1 as stated in the introduction is known to bind GSH via the conserved cystine 24 residue. This cystine sits in a binding 'pocket' in CLIC1 as shown in the diagram above, this pocket displays a high amount of chemical shift when GSH binds. However, there are significant amounts of chemical shift throughout the protein even in areas not in close proximity to this binding site.

10.5 Analysis of GSTO1 GSH binding site when complexing with GSH saturated peptide:

In vivo GSTO1 is thought to have a role in the glutathione cycle more specifically deglutathionylating cystines 'capped' with GSH and stated in the introduction. Meaning GSTO1 does not interact with free GSH in cell but GSH attached to compounds. For this reason, an experiment was derived to see if GSTO1 not only interacts with the GSH but also potentially has an interaction with the compound GSH is attached to. A small polypeptide (SQLWCLSN) was saturated with GSH to produce (SQLWC^{GSH}LSN). Then the same titration used in the first part of this chapter was carried out. The results of which can be seen below in figure 20.

GSTO1 titration with peptide saturated with glutathione (GSH)

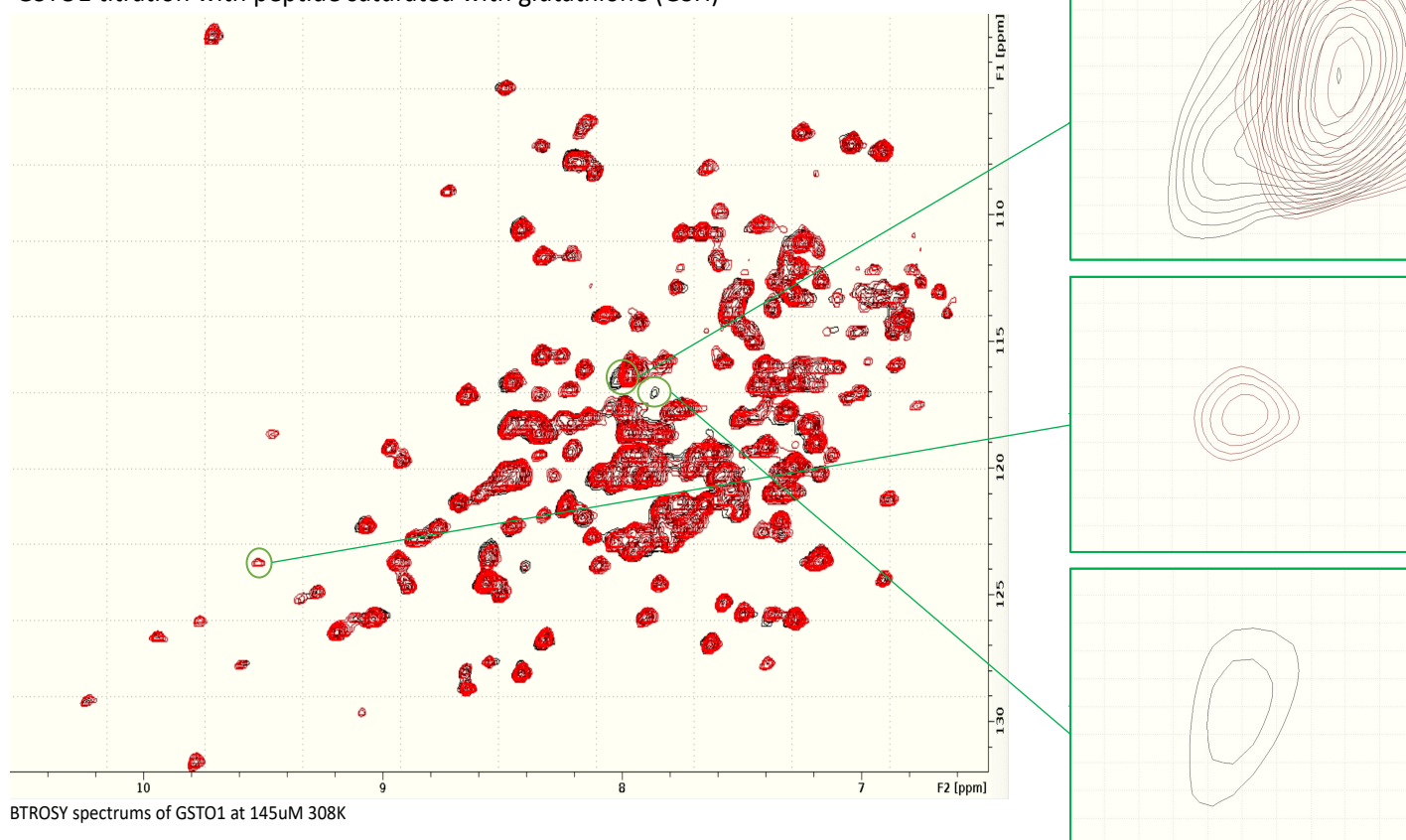


Figure 20: BEST TROSY HSQC spectra of GSTO1 at 145uM, 308K, pH 7.4, 20mM NaCl, 20mM Phosphate.

Two spectra aligned and overlaid with each other. A 0 molar ratio of GSH in red, a 1 molar ratio in black.

Here we see some peak shifting and intensity change but this time some of these resonances are in slow exchange. Unfortunately, due to the lack of assignment we cannot compare the titration data of GSTO1 with free GSH and the peptide saturated with GSH to see if there are any residues shifting more or less, or any extra residues shifting as we don't know which peaks correspond to which residues due to the lack of assignment.

11 Discussion

CLIC1 has long been known to be a structural homologue of GSTO1³⁷, the CLIC family of proteins are also known to be metamorphic and able to insert into the membrane and oligomerise to form an ion channel^{48,65}. GSTO1 does not have metamorphic properties and only exists in a soluble form, it does however have strong enzymatic properties which CLIC1 lacks^{10,37}. The aim of this project using both computational and experimental analysis is to try and better understand how CLIC1 can have these vastly different functions to GSTO1 despite the high homology.

11.1 Differences in X-ray crystal structure:

The sequence alignment done in figure 5 shows a relatively low sequence identity at 19.1% however, many the amino acids that are not fully conserved are either strongly or weakly conserved via their properties. This is evidenced by the very high homology in the X-ray crystal structure alignment shown in figure 6. The overall structure is clearly the same with both having a C-domain full of alpha helixes and a N-domain containing the thioredoxin-like domain and the catalytic cystine residue C32 for GSTO1 and C24 for CLIC1. Despite these overarching similarities there are some interesting disparities found in the crystal structure which could explain the very different function of the two proteins. Two of the major differences being the proline rich ‘footloop’ and the shifted H9 helix, both of which will be expand upon further below.

11.2 Elucidating the in-Solution Structures and Conformational Dynamics of GSTO1 and CLIC1 using SAXS:

The SAXS experiments performed to try and gain insight into the in-solution structures provided some interesting results. When looking at the crystal structures for GSTO1 and CLIC1 they appear extremely similar as would be expected of structural homologues. However, looking at the SAXS data shown in figure 7 it is clear that while GSTO1's in-solution structure matches that of its crystal structure with a chi squared score of 1.26 for the fit. The same cannot be said for CLIC1 which has a chi squared score of 5.14. This suggests that the crystal structure for CLIC1 is not the shape it is adopting in-solution. This is compounded by the results from figure 8 showing a P(r) plot of both proteins. As has been stated above GSTO1's bell shaped curve which is indicative of a globular protein supports the shape of its crystal structure CLIC1's does not. The P(r) plot for CLIC1 has a 'tail' implying a certain amount of disorder in the protein, something not commonly found in globular proteins. This disorder is shown in the B factor analysis figures 8-11 where CLIC1 has higher disorder in certain key areas of the protein such as the 'footloop' than GSTO1. It is also shown in the NMR spin relaxation experiment that the 'footloop' (residues 41-61) disorder is not fast backbone movements (ps-ns) but slow backbone movements (us-ms). These slow movements are often associated with conformational change. Therefore, one explanation for the difference in in-solution structure could be this 'footloop' providing the flexibility for CLIC1 to change shape in-solution and GSTO1 remaining globular.

11.3 Structural disorder and intramolecular bonding in GSTO1 and CLIC1:

B-factor analysis of both GSTO1 and CLIC1 shows areas of higher disorder in CLIC1. Although the average disorder in GSTO1 is greater, this is due to the lower resolution X-ray crystal structure. Figures 8 and 9 show these areas of high disorder in CLIC1 particularly residues 41-61, 88-100 and 147-164. The same areas do not exhibit the same disorder in GSTO1 as shown in figures 10 and 11. The NMR spin relaxation experiment showing CLIC1s backbone movements (figure 13) experientially backs up the B-factor analysis and shows these same areas of disorder are conserved when the protein is in-solution.

As well as having areas of higher disorder CLIC1 also has fewer intramolecular bonds between its two domains the C and N-domain. This can be seen in tables 1 and 2 showing CLIC1 having half the amount of intramolecular bonds (30) that GSTO1 possesses (60). CLIC1 also has two fewer types of interactions as well lacking both the Aromatic-Aromatic interactions and Aromatic-Sulphur interactions that GSTO1 has. The Thermofluor experiments carried out also experimentally back up the intramolecular bond analysis, showing GSTO1 to have a higher T_m (60-62°C) than that of CLIC1 (55-58°C) (figures 14 and 15) as with fewer intramolecular bonds holding the two subunits together it takes less energy to denature CLIC1 and therefore the T_m is lower. One interesting thing to note from figure 14 and 15 is the difference between GSTO1, un-cleaved CLIC1 and cleaved CLIC1s transition peaks. CLIC1 with a cleaved his-tag has two transitions peaks whereas, un-cleaved CLIC1 and GSTO1 only has one. It is known that the his-tag being left on CLIC1 stops oligomerisation and membrane insertion. Therefore, potentially the two transition peaks we are seeing in figure 14 are one for the CLIC1 in its soluble state resembling GSTO1 and another for the conformation that the SAXS data is suggesting.

The fewer intramolecular interactions combined with the higher disorder in certain areas of CLIC1 would allow for more flexibility in the protein, potentially allowing it to shift from the globular X-ray crystal structure, which CLIC1 must do before it inserts into the membrane.

11.4 Comparison of the GSH binding site on GSTO1 and CLIC1:

Figures 15 and 16 are of NMR titration experiments showing GSTO1 and CLIC1 complexing with GSH as evidenced by the clear shifting of peaks and changes in intensity when GSH is titrated into the sample. Visually from the spectra GSTO1 appears to have both a greater number of peaks shifting and this shifting being of higher ppm than CLIC1. This aligns with the knowledge that GSTO1 is an enzyme that binds GSH as its substrate, and CLIC1 is not known to have these same strong enzymatic properties. Unfortunately, due to the lack of assignment of GSTO1 we cannot directly compare these two data sets as we cannot know which exact residues are shifting in GSTO1 and by how much.

Whilst we do not have GSTO1 assigned we do have CLIC1 assigned. This means we can see exactly which residues in CLIC1 shifted when GSH was added and how much they shifted. The shift in ppm for each residue in CLIC1 can be seen in figure 18 and is visualised in the crystal structure 1k0m in figure 19. These figures show the greatest amount of chemical shift around the binding pocket where cysteine 24 interacts with GSH however, there are significant amounts of chemical shift all over the protein.

Figure 20 shows an NMR titration of GSTO1 with GSH saturated peptide. The aim of this experiment was to look for differences in peak shifting between GSTO1 binding free GSH and binding GSH bound to a peptide. The hope was to see if there were any allosteric binding

sites on GSTO1 where the peptide may interact. Again, unfortunately due to the lack of assignment we cannot directly compare the peak shifting of the two experiments shown in figure 16 and 20, to see if the same residues are shifting the same amount or if there are any new areas of chemical shift.

11.5 The Footloop hypothesis:

One of the main differences in structure is the ‘footloop’ connecting the two domains in CLIC1 and GSTO1. This ‘footloop’ is found between helices H5 and H6 and in CLIC1 is greatly elongated compared to GSTO1. Interestingly the B-factor analysis shown in figures 8 and 9 of this loop showed a high above average B-factors for this loop in CLIC1, indicating it as an area of high flexibility due to disorder in the crystal structure. When the same analysis was done on the loop connecting GSTO1’s two domains shown in figures 10 and 11 it was not found as an area above the average B-factor and therefore was not indicated as an area of high flexibility.

Whilst B-factors can give good insight into areas of potential flexibility in proteins it is computational and therefore not experimental data. The NMR spin relaxation experiment shown in figure 13 supports the computational data of the B-factors, as in previous studies areas with a hinge bending motion generally have a slow backbone movement at the microsecond to millisecond (μs - ms). This can be seen in figure 13 with the ‘footloop’, giving more weight to the hypothesis that the ‘footloop’ connecting CLIC1’s two domains could act as a hinge allowing for conformational shift. This could explain how GSTO1 is a globular relatively static enzyme and CLIC can undergo conformational changes and insert into the membrane despite the seemingly high structural homology. An interesting thing to note that

in the literature proline rich loops such as the ‘footloop’ in CLIC1 normally have high rigidity, CLIC1 appears to be an exception to this.

The hypothesis of the ‘footloop’ acting as a hinge is further supported by the intramolecular bond analysis. Tables 1 and 2 shows the total number of interactions between the two domains in both CLIC1 and GSTO1. GSTO1 has double the total amount of intramolecular interactions between the two subunits as well as two extra types of intramolecular interactions. This would be consistent with GSTO1 being a globular enzyme in the solute and CLIC1 have the ability to undergo conformational change and insert into the membrane.

The Thermofluor analysis shown in figure 14 and 15 displays GSTO1 having a T_m of 60-62°C which is higher than CLIC1’s T_m of 57°C. This reinforces the computational intramolecular bond analysis as you would expect less bonding between the subunits to lower the T_m of the protein. This lowered T_m makes sense in the context of a less globular and more dynamic protein, as more dynamics requires more freedom in terms of movement in the backbone therefore a greater density of bonds in a protein is disadvantageous to this.

11.6 The H9 helix hypothesis:

The other major difference in crystal structure between GSTO1 and CLIC1 is the shifted H9 helix. This helix forms as the ‘lid’ of the H binding site, in CLIC1 the H site is more elongated and open than in GSTO1 hence why the H9 helix is shifted as shown in figure 6⁷⁶. It is known that CLIC1 can bind cations such as Zn^{2+} and Ca^{2+} and in insect homologues of

CLIC1 this site is found overlapping the GSH binding site of GSTO1⁶⁷. One reason for this shift in the H9 helix could be to allow for this cation binding site.

11.7 Limitations:

A triple labelled backbone assignment NMR experiment was attempted for GSTO1. This was unsuccessful as GSTO1 is a large 55kDa dimer in solution, it is also very globular. These characteristics make GSTO1 a difficult protein to study using NMR due to a slow tumble and very slow exchange in the centre of the protein. With a few more months I believe that high enough quality results could have been achieved to successfully perform the assignment. The lack of this data severely affected comparisons we could conduct with out titration data.

11.8 Further research:

Obtaining the assignments for GSTO1 would allow for greater comparison between GSTO1 and CLIC1s interactions with GSH and general enzymatic activity. As there is evidence for cation binding causing the conformational shift allowing CLIC1 to insert into the membrane, a similar NMR titration experiment could be carried out for CLIC1, but instead of using GSH as the ligand a cation such as Zn^{2+} could be used. This titration could then be compared to GSTO1 and CLIC1s titration with GSH. If the cation binding does cause a conformational shift in CLIC1 these areas will show on the CLIC1 titration with Zn^{2+} but not on GSTO1 or CLIC1s titration with GSH as this complex does not cause insertion into the membrane. These areas of the protein could be further studied to try and understand more about the mechanism of CLIC1 membrane insertion.

12 Conclusions

In summary from the data gathered it is clear that while GSTO1 and CLIC1s X-ray crystal structures are very similar this changes when both proteins are put into solution. While GSTO1 X-ray crystal structure is indicative of its in-solution structure CLIC1s is not, the SAXS data shows CLIC1 does not adopt this globular structure but instead something more disordered. This different shape is likely facilitated by the extended proline rich 'footloop' found in CLIC1 which may act as a hinge allowing for conformational change. This would fit with the current literature as CLIC1 is a metamorphic protein and is known to adopt two distinct structures. Furthermore, the shifted H9 helix could be to accommodate a cation binding site in CLIC1. The enzymatic differences between the two proteins are less clear due to the lack of assignment in GSTO1 stopping direct comparison of chemical shift in the protein. However, looking at the spectra visually there are some clear differences which could be confirmed once the assignment has been obtained.

13 References

1. Board, P. G. *et al.* Identification, Characterization, and Crystal Structure of the Omega Class Glutathione Transferases *. *Journal of Biological Chemistry* **275**, 24798–24806 (2000).
2. Oakley, A. J. Glutathione transferases: new functions. *Curr Opin Struct Biol* **15**, 716–723 (2005).
3. Sheehan, D., Meade, G., Foley, V. M. & Dowd, C. A. Structure, function and evolution of glutathione transferases: implications for classification of non-mammalian members of an ancient enzyme superfamily. *Biochem J* **360**, 1–16 (2001).
4. Hayes, J. D., Flanagan, J. U. & Jowsey, I. R. Glutathione transferases. *Annu Rev Pharmacol Toxicol* **45**, 51–88 (2005).
5. Oakley, A. Glutathione transferases: a structural perspective. *Drug Metab Rev* **43**, 138–51 (2011).
6. Ladner, J. E., Parsons, J. F., Rife, C. L., Gilliland, G. L. & Armstrong, R. N. Parallel evolutionary pathways for glutathione transferases: structure and mechanism of the mitochondrial class kappa enzyme rGSTK1-1. *Biochemistry* **43**, 352–361 (2004).
7. Robinson, A., Huttley, G. A., Booth, H. S. & Board, P. G. Modelling and bioinformatics studies of the human Kappa-class glutathione transferase predict a novel third glutathione transferase family with similarity to prokaryotic 2-hydroxychromene-2-carboxylate isomerases. *Biochem J* **379**, 541–552 (2004).
8. Jakobsson, P.-J., Morgenstern, R., Mancini, J., Ford-Hutchinson, A. & Persson, B. Common structural features of MAPEG -- a widespread superfamily of membrane associated proteins with highly divergent functions in eicosanoid and glutathione metabolism. *Protein Science : A Publication of the Protein Society* **8**, 689 (1999).
9. Atkinson, H. J. & Babbitt, P. C. Glutathione Transferases Are Structural and Functional Outliers in the Thioredoxin Fold. *Biochemistry* **48**, 11108–11116 (2009).
10. Armstrong, R. N. Structure, Catalytic Mechanism, and Evolution of the Glutathione Transferases. *Chemical Research in Toxicology* **10**, 2–18 (1997).
11. DIRR, H., REINEMER, P. & HUBER, R. X-ray crystal structures of cytosolic glutathione S-transferases. Implications for protein architecture, substrate recognition and catalytic function. *Eur J Biochem* **220**, 645–661 (1994).
12. Ishikawa, T. The ATP-dependent glutathione S-conjugate export pump. *Trends Biochem Sci* **17**, 463–468 (1992).
13. Eaton, D. L. & Bammler, T. K. Concise review of the glutathione S-transferases and their significance to toxicology. *Toxicological Sciences* **49**, 156–164 (1999).
14. Bhakta, K. Y., Adams, J. M. & Stark, A. R. Chronic lung disease of infancy. *Pulmonary Manifestations of Paediatric Diseases* 1–27 (2009) doi:10.1016/B978-1-4160-3031-7.00001-2.
15. Hayes, P. C., Bouchier, A. D. & Beckett, G. J. Glutathione S-transferase in humans in health and disease. *Gut* **32**, 813–818 (1991).
16. Ray, P. D., Huang, B. W. & Tsuji, Y. Reactive oxygen species (ROS) homeostasis and redox regulation in cellular signalling. *Cell Signal* **24**, 981 (2012).
17. Auten, R. L. & Davis, J. M. Oxygen Toxicity and Reactive Oxygen Species: The Devil Is in the Details. *paediatric Research* 2009 66:2 **66**, 121–127 (2009).
18. Turrens, J. F. Mitochondrial formation of reactive oxygen species. *The Journal of Physiology* **552**, 335 (2003).
19. Li, X. *et al.* Targeting mitochondrial reactive oxygen species as novel therapy for inflammatory diseases and cancers. *Journal of Haematology & Oncology* **6**, 19 (2013).

20. Poljsak, B., Šuput, D. & Milisav, I. Achieving the balance between ROS and antioxidants: When to use the synthetic antioxidants. *Oxidative Medicine and Cellular Longevity* (2013) doi:10.1155/2013/956792.
21. Muthukumar, K. & Nachiappan, V. Cadmium-induced oxidative stress in *Saccharomyces cerevisiae*. *Indian J Biochem Biophys* **47**, 383–7 (2010).
22. Guengerich, F. P. Enzymatic oxidation of xenobiotic chemicals. *Crit Rev Biochem Mol Biol* **25**, 97–153 (1990).
23. Ishikawa, T. The ATP-dependent glutathione S-conjugate export pump. *Trends Biochem Sci* **17**, 463–8 (1992).
24. Salinas, A. E. & Wong, M. G. Glutathione S-transferases--a review. *Curr Med Chem* **6**, 279–309 (1999).
25. Hayes, J. D. & McLellan, L. I. Glutathione and glutathione-dependent enzymes represent a co-ordinately regulated defence against oxidative stress. *Free Radic Res* **31**, 273–300 (1999).
26. Pajaud, J., Kumar, S., Rauch, C., Morel, F. & Aninat, C. Regulation of Signal Transduction by Glutathione Transferases. *International Journal of Hepatology* **2012**, 1–11 (2012).
27. Wongtrakul, J., Sukittikul, S., Saisawang, C. & Ketterman, A. J. Mitogen-Activated Protein Kinase p38b Interaction with Delta Class Glutathione Transferases from the Fruit Fly, *Drosophila melanogaster*. *Journal of Insect Science* **12**, 107 (2012).
28. Thévenin, A. F., Zony, C. L., Bahnson, B. J. & Colman, R. F. GST pi modulates JNK activity through a direct interaction with JNK substrate, ATF2. *Protein Sci* **20**, 834–848 (2011).
29. Ip, Y. T. & Davis, R. J. Signal transduction by the c-Jun N-terminal kinase (JNK)--from inflammation to development. *Curr Opin Cell Biol* **10**, 205–219 (1998).
30. Josephy, P. D. Genetic Variations in Human Glutathione Transferase Enzymes: Significance for Pharmacology and Toxicology. *Human Genomics and Proteomics : HGP* **2010**, 14 (2010).
31. Shahid, P. B. A. B. Role of thiols in oxidative stress. *Current Opinion in Toxicology* **7**, 133–139 (2018).
32. Menon, D. & Board, P. G. A Role for Glutathione Transferase Omega 1 (GSTO1-1) in the Glutathionylation Cycle. *The Journal of Biological Chemistry* **288**, 25769 (2013).
33. Whitbread, A. K. *et al.* Characterization of the omega class of glutathione transferases. *Methods Enzymol* **401**, 78–99 (2005).
34. GSTO1 glutathione S-transferase omega 1 [Homo sapiens (human)] - Gene - NCBI. <https://www.ncbi.nlm.nih.gov/gene/9446>.
35. Meng, F., Zhang, Y., Liu, F., Guo, X. & Xu, B. Characterization and Mutational Analysis of Omega-Class GST (GSTO1) from *Apis cerana cerana*, a Gene Involved in Response to Oxidative Stress. *PLoS ONE* **9**, e93100 (2014).
36. Opitz, R. *et al.* A modular toolkit to inhibit proline-rich motif-mediated protein-protein interactions. *Proc Natl Acad Sci U S A* **112**, 5011–5016 (2015).
37. Dulhunty, A., Gage, P., Curtis, S., Chelvanayagam, G. & Board, P. The Glutathione Transferase Structural Family Includes a Nuclear Chloride Channel and a Ryanodine Receptor Calcium Release Channel Modulator. *Journal of Biological Chemistry* **276**, 3319–3323 (2001).
38. Goodchild, S. C., Angstmann, C. N., Breit, S. N., Curmi, P. M. G. & Brown, L. J. Transmembrane extension and oligomerization of the CLIC1 chloride intracellular channel protein upon membrane interaction. *Biochemistry* **50**, 10887–97 (2011).

39. Dulhunty, A. F., Hewawasam, R., Liu, D., Casarotto, M. G. & Board, P. G. Regulation of the cardiac muscle ryanodine receptor by glutathione transferases. *Drug Metab Rev* **43**, 236–52 (2011).
40. Valenzuela, S. M. *et al.* Molecular cloning and expression of a chloride ion channel of cell nuclei. *J Biol Chem* **272**, 12575–12582 (1997).
41. Heiss, N. S. & Poustka, A. Genomic structure of a novel chloride channel gene, CLIC2, in Xq28. *Genomics* **45**, 224–228 (1997).
42. Qian, Z., Okuhara, D., Abe, M. K. & Rosner, M. R. Molecular cloning and characterization of a mitogen-activated protein kinase-associated intracellular chloride channel. *J Biol Chem* **274**, 1621–1627 (1999).
43. Duncan, R. R., Westwood, P. K., Boyd, A. & Ashley, R. H. Rat brain p64H1, expression of a new member of the p64 chloride channel protein family in endoplasmic reticulum. *J Biol Chem* **272**, 23880–23886 (1997).
44. Howell, S., Duncan, R. R. & Ashley, R. H. Identification and characterisation of a homologue of p64 in rat tissues. *FEBS Lett* **390**, 207–210 (1996).
45. Berryman, M. & Bretscher, A. Identification of a novel member of the chloride intracellular channel gene family (CLIC5) that associates with the actin cytoskeleton of placental microvilli. *Mol Biol Cell* **11**, 1509–1521 (2000).
46. Nishizawa, T., Nagao, T., Iwatsubo, T., Forte, J. G. & Urushidani, T. Molecular cloning and characterization of a novel chloride intracellular channel-related protein, parchorin, expressed in water-secreting cells. *J Biol Chem* **275**, 11164–11173 (2000).
47. Murzin, A. G. Biochemistry: Metamorphic proteins. *Science (1979)* **320**, 1725–1726 (2008).
48. Goodchild, S. C. *et al.* Metamorphic response of the CLIC1 chloride intracellular ion channel protein upon membrane interaction. *Biochemistry* **49**, 5278–89 (2010).
49. Littler, D. R. *et al.* The enigma of the CLIC proteins: Ion channels, redox proteins, enzymes, scaffolding proteins? *FEBS Lett* **584**, 2093–101 (2010).
50. Ulmasov, B., Bruno, J., Woost, P. G. & Edwards, J. C. Tissue and subcellular distribution of CLIC1. *BMC Cell Biology* **8**, 8 (2007).
51. Valenzuela, S. M. *et al.* Molecular cloning and expression of a chloride ion channel of cell nuclei. *J Biol Chem* **272**, 12575–12582 (1997).
52. Liu, B. *et al.* Chloride intracellular channel 1 (CLIC1) contributes to modulation of cyclic AMP-activated whole-cell chloride currents in human bronchial epithelial cells. *Physiol Rep* **6**, (2018).
53. Harrop, S. J. *et al.* Crystal structure of a soluble form of the intracellular chloride ion channel CLIC1 (NCC27) at 1.4-Å resolution. *J Biol Chem* **276**, 44993–45000 (2001).
54. Khamici, H. *al et al.* Members of the Chloride Intracellular Ion Channel Protein Family Demonstrate Glutaredoxin-Like Enzymatic Activity. *PLoS ONE* **10**, 115699 (2015).
55. Jones, P. M., Curmi, P. M. G., Valenzuela, S. M. & George, A. M. Computational analysis of the soluble form of the intracellular chloride ion channel protein CLIC1. *Biomed Res Int* **2013**, (2013).
56. Wu, X. & Rapoport, T. A. Cryo-EM structure determination of small proteins by nanobody-binding scaffolds (Legobodies). *Proc Natl Acad Sci U S A* **118**, (2021).
57. Gopinath, T., Weber, D., Wang, S., Larsen, E. & Veglia, G. Solid-State NMR of Membrane Proteins in Lipid Bilayers: To Spin or Not To Spin? *Accounts of Chemical Research* **54**, 1430–1439 (2021).
58. Littler, D. R. *et al.* The intracellular chloride ion channel protein CLIC1 undergoes a redox-controlled structural transition. *J Biol Chem* **279**, 9298–305 (2004).

59. Ulmasov, B. *et al.* CLIC1 null mice demonstrate a role for CLIC1 in macrophage superoxide production and tissue injury. *Physiol Rep* **5**, (2017).
60. He, G. *et al.* Role of CLIC4 in the host innate responses to bacterial lipopolysaccharide. *Eur J Immunol* **41**, 1221–30 (2011).
61. Bradford, E. M. *et al.* CLIC5 mutant mice are resistant to diet-induced obesity and exhibit gastric haemorrhaging and increased susceptibility to torpor. *Am J Physiol Regul Integr Comp Physiol* **298**, R1531-42 (2010).
62. Goodchild, S. C. *et al.* Oxidation promotes insertion of the CLIC1 chloride intracellular channel into the membrane. *Eur Biophys J* **39**, 129–38 (2009).
63. Valenzuela, S. M. *et al.* Regulation of the Membrane Insertion and Conductance Activity of the Metamorphic Chloride Intracellular Channel Protein CLIC1 by Cholesterol. *PLOS ONE* **8**, e56948 (2013).
64. Varela, L. C. H. A. C. J. M.-E. R. C. E. J. A.-S. V. O.-R. L. Zn²⁺ triggered two-step mechanism of CLIC1 membrane insertion and activation into chloride channels. *bioRxiv* (2021).
65. Varela, L. C. H. A. C. D. L. O.-R. J. The membrane insertion of soluble CLIC1 into active chloride channels is triggered by specific divalent cations. *bioRxiv* (2019).
66. Stoychev, S. H. *et al.* Structural Dynamics of Soluble Chloride Intracellular Channel Protein CLIC1 Examined by Amide Hydrogen–Deuterium Exchange Mass Spectrometry. *Biochemistry* **48**, 8413–8421 (2009).
67. Littler, D. R. *et al.* Comparison of vertebrate and invertebrate CLIC proteins: the crystal structures of *Caenorhabditis elegans* EXC-4 and *Drosophila melanogaster* DmCLIC. *Proteins* **71**, 364–78 (2008).
68. Setti, M. *et al.* Functional role of CLIC1 ion channel in glioblastoma-derived stem/progenitor cells. *J Natl Cancer Inst* **105**, 1644–55 (2013).
69. Wang, W. *et al.* The expression and clinical significance of CLIC1 and HSP27 in lung adenocarcinoma. *Tumor Biology* **32**, 1199–1208 (2011).
70. Zhang, J. *et al.* Clc1 plays a role in mouse hepatocarcinoma via modulating Annexin A7 and Gelsolin in vitro and in vivo. *Biomedicine & pharmacotherapy = Biomedecine & pharmacotherapie* **69**, 416–9 (2015).
71. Chen, C.-D. *et al.* Overexpression of CLIC1 in human gastric carcinoma and its clinicopathological significance. *PROTEOMICS* **7**, 155–167 (2007).
72. Clustal Omega < Multiple Sequence Alignment < EMBL-EBI. <https://www.ebi.ac.uk/Tools/msa/clustalo/>.
73. The PyMOL Molecular Graphics System, V. 2. 0 S. LLC. PyMOL. (2021).
74. Craig, D. B. & Dombkowski, A. A. Disulfide by Design 2.0: A web-based tool for disulfide engineering in proteins. *BMC Bioinformatics* **14**, (2013).
75. Tina, K. G., Bhadra, R. & Srinivasan, N. PIC: Protein Interactions Calculator. *Nucleic Acids Research* **35**, (2007).
76. Wang, W. *et al.* Identification of Potent Chloride Intracellular Channel Protein 1 Inhibitors from Traditional Chinese Medicine through Structure-Based Virtual Screening and Molecular Dynamics Analysis. *Biomed Res Int* **2017**, 4751780 (2017).